DALHOUSIE UNIVERSITY

Fillet welds around circular hollow sections

Kyle Tousignant[a*] and Jeffrey A. Packer[b]

[a] Department of Civil and Resource Engineering, Dalhousie University, Sexton Campus, 1360 Barrington Street, Halifax, NS, B3H 4R2, Canada

[b] Department of Civil & Mineral Engineering, University of Toronto, 35 St. George Street, Toronto, ON, M5S 1A4, Canada

[*] Corresponding Author. E-mail: kyle.tousignant@dal.ca; Tel: +1-902-494-3080; ORCID: 0000-0001-5975-7532

Abstract

An experimental and numerical research program was conducted to evaluate the safety of North American design rules for fillet welds around the perimeter of steel circular hollow sections (CHS). This assessment was performed in the context of the current American Institute of Steel Construction (AISC) steel building specification, AISC 360. Specifically, the appropriateness of the fillet weld directional strength-enhancement factor in AISC 360-16 Clause J2.4b was investigated for fillet welds to CHS branches, and the effect of non-uniform connection flexibility on the strength of welds in CHS-to-CHS connections was studied. A total of 24 large-scale, weld-critical experiments was tested and a further 290 non-linear finite element models were used to parametrically expand the database. It was found that if the directional-strength factor is used the target reliability (or safety) index prescribed by AISC for connectors, even when the welds are fully effective, is not achieved; hence, a recommendation to prohibit this factor for all fillet welds around the perimeter of CHS is made. With this restriction, it is then shown that AISC 360-16 Clause J2.4a fillet weld design provisions meet AISC's target safety index for welds in CHS-to-CHS X-connections, where a weld effective length phenomenon exists. It is therefore recommended that AISC advocate 100% weld effective lengths for fillet welds in CHS-to-CHS X-connections, provided that the directional strength-enhancement factor ($1.0+0.5\sin^{1.5}\theta$) is not used.

Key words

Circular hollow section, Fillet weld, Effective length, Connection, Experiment, Finite element

1. Introduction

When welding to hollow structural sections (HSS), welds can be proportioned either: (a) to achieve the capacity of the connected branch member walls, or (b) to be "fit-for-purpose", by considering weld effective lengths (or properties) [1]. By designing welds as "fit-for-purpose" – to resist the actual forces present in the branch member – smaller, more appropriate, and still safe weld sizes can often result.

Over the past 30 years, substantial experimental research efforts have focused on determining weld effective lengths for rectangular hollow section (RHS) connections, including gapped K-connections, T-, Y- and X- (or Cross-) connections, moment-loaded T-connections, and overlapped K-connections [2-6]. Recommendations based on this research have been adopted in North America, by the American Institute of Steel Construction (AISC) in Section K5: "Welds of Plates and Branches to Rectangular HSS" of their latest (2016) steel building specification [7].

When using the weld effective length rules in AISC 360-16 Section K5 to design fillet welds to RHS, the fillet weld directional strength-enhancement factor ($1.0+0.5\sin^{1.5}\theta$) in Clause J2.4b should not be used (i.e. it has been shown, experimentally, that target reliability levels are not achieved) [5, 6, 8-10].

Since the addition of Section K5 (formerly Section K4, in the 2010 specification [11]), weld effective lengths for circular hollow section (CHS) connections have been an issue faced by many code writers, including AISC, since load transfer around a CHS branch can be highly non-uniform [12]. Moreover, the applicability of the ($1.0+0.5\sin^{1.5}\theta$) factor to fillet welds around the perimeter of CHS is unverified. This includes fillet welds in CHS-to-CHS connections, and even fillet welds in CHS-to-rigid plate connections (where the entire weld length is effective), since in both cases bending about the weld axis is unrestrained.

A total of 24 large-scale, weld-critical experiments and 290 non-linear finite element (FE) models was hence investigated to assess the strength of fillet welds around CHS branches, beginning with the applicability of the ($1.0+0.5\sin^{1.5}\theta$) factor to fillet welds in CHS-to-rigid plate connections (Fig. 1a). Weld-critical tests on large-scale, fillet-welded, CHS-to-CHS X-connections (Fig. 1b) were then conducted, and corresponding FE models were developed to determine the adequacy of current AISC 360-16 Section J2.4 weld design provisions.

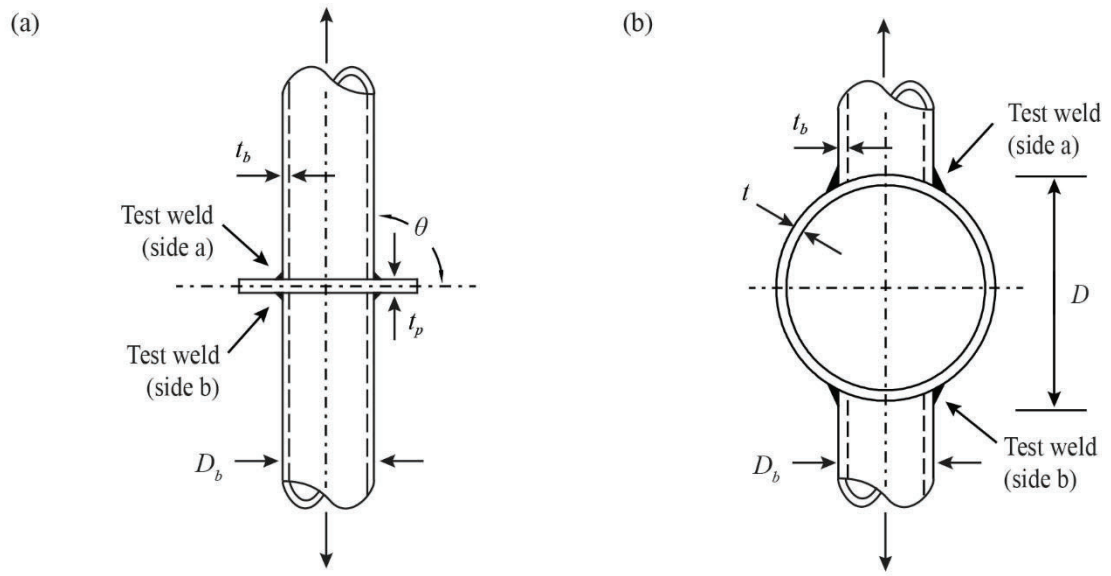

Fig. 1 Experimental test specimens: (a) CHS-to-rigid plate connection; (b) CHS-to-CHS X-connection

2. Fillet welds in CHS-to-rigid plate connections: experiments

2.1. Mechanical and geometrical properties

Six CHS-to-rigid plate connections (Fig. 1a), comprising 12 weld-critical experiments (two per connection), were fabricated from cold-formed CHS made to ASTM A500 Grade C [13] and 25-mm plate with a nominal yield strength of 350 MPa. Fillet welds were made using a semi-automatic flux-cored-arc-welding (FCAW) process with CO_2 shielding gas and an E71T-1C electrode. The average yield stress (F_y) and ultimate stress (F_u, or F_{EXX} for the weld metal) of the CHS, plate and weld metal, determined by tensile coupon testing in accordance with ASTM A370 [14] or AWS D1.1 [15] (for the weld metal) are summarized in Table 1.

Table 1. Measured material properties for the 12 CHS-to-rigid plate experiments

	CHS branch		Plate		Weld metal	
Test No.	F_y MPa	F_u MPa	F_y MPa	F_u MPa	F_y MPa	F_{EXX} MPa
P1, P2, P7, and P8	421	501	409	566	501	571
P3, P4, P9, and P10	431	488	409	566	501	571
P5, P6, P11, and P12	385	450	409	566	501	571

Trial welds were made (prior to fabrication) on identical joints to the CHS-to-rigid plate connections and thereafter sectioned to (a) ensure adequate fusion and (b) set the welding process specification (WPS) for the test connections. A WPS was chosen, from those tested, to produce minimal but just-adequate weld root penetration to allow for accurate characterization of the weld throat dimension(s) (t_w).

Prior to testing, fillet weld faces were ground flat, and leg dimensions on the branch and plate (l_v and l_h) were measured at uniform increments ≤ 30 mm around the CHS perimeter using standard (90° or skew-T) fillet weld gauges. For each pair of leg measurements, t_w was calculated using Eq. (1). Eq. (1) takes into account the effect of unequal leg sizes and the local dihedral angle, ψ (i.e. the angle between the base metal fusion faces), on the orientation of the weld throat plane. For the $\theta = 90°$ connections, $\Psi = 90°$ around the entire joint. For the $\theta = 60°$ connections, Ψ varies continuously around the joint, and it was determined using a method by Luyties & Post [16], programmed in Matlab with measured dimensions of the CHS. In both cases, weld root penetration was ignored because it was shown to be minimal for the chosen WPS.

$$t_w = \frac{l_v l_h \sin\psi}{\sqrt{l_v^2 + l_h^2 - 2 l_v l_h \cos\psi}} \tag{1}$$

The total weld length (l_w), which is used to calculate the weld throat area ($A_w = t_w l_w$), was taken as the CHS contact perimeter, and hence measured along the root of the weld considering the angle between the CHS and the plate. The CHS-to-plate test connection parameters are summarized in Table 2.

Table 2. Measured geometric properties and ultimate loads (experimental and FE) for $\theta = 90°$ and $\theta = 60°$ CHS-to-rigid plate experiments

Test no.	θ	CHS dimensions $D_b \times t_b$	t_p	l_w	Average weld dimensions t_w	l_v	l_h	P_a'	P_{FE}	P_a'/P_{FE}
	°	mm × mm	mm	mm	mm	mm	mm	kN	kN	
P1	90	167.9 × 6.70	25.0	528	4.81	7.04	6.60	1261	1210	1.04
P2					6.63	9.64	9.13	1279	1523	0.84
P3	90	127.4 × 11.55	25.0	401	6.87	9.89	9.54	1459	1337	1.09
P4					7.98	11.23	11.34	1597	1530	1.04
P5	90	101.0 × 7.34	25.0	318	6.38	8.85	9.22	841	860	0.98
P6					6.16	9.23	8.28	864	877	0.99
P7	60	167.9 × 6.70	25.0	569	5.32	6.13	7.41	1450	1207	1.20
P8					5.73	6.88	7.71	1331	1324	1.01
P9	60	127.4 × 11.55	25.0	432	5.21	8.06	8.54	1109	1278	0.87
P10					6.78	10.50	11.13	1479	1601	0.92
P11	60	101.0 × 7.34	25.0	342	5.39	6.93	7.75	776	763	1.02
P12					4.98	6.71	7.32	803	743	1.08

Note: P_a' = greatest actual (experimental) load sustained by the weld; P_{FE} = failure load in the finite element model.

2.2. Test set-up, instrumentation, and results

Quasi-static tension was applied to the ends of the CHS branches by an MTS universal testing machine (UTM), and weld displacement, over a 50-mm gage length, and branch axial strains were measured (Fig. 2a). The branch axial strains were measured at two locations along the branch length: (1) adjacent to the weld, 20 mm from the vertical toe; and (2) in the constant stress region identified by Mehrotra & Govil [17] – a distance of $3D_b$ from the weld toe. These measured strain values were uniform throughout the majority of the tests, indicating that:

(1) the entire weld length was effective (there was uniform loading of the weld); and

(2) the specimens were loaded in pure tension (i.e. there were no bending moments caused by misalignments in the test set-up or by test specimen out-of-straightness).

All 12 test joints failed by weld rupture along a plane through the weld (Fig. 2b). After rupture of one test weld in each connection (e.g. side a), the entire specimen was removed from the UTM and fully re-welded (nominally in the flat position) to ensure separation of the same branch did not occur again. The connection was then tested again, until rupture of the second test weld (e.g. side b) occurred. The ultimate (weld rupture) loads (P_a') are given in Table 2.

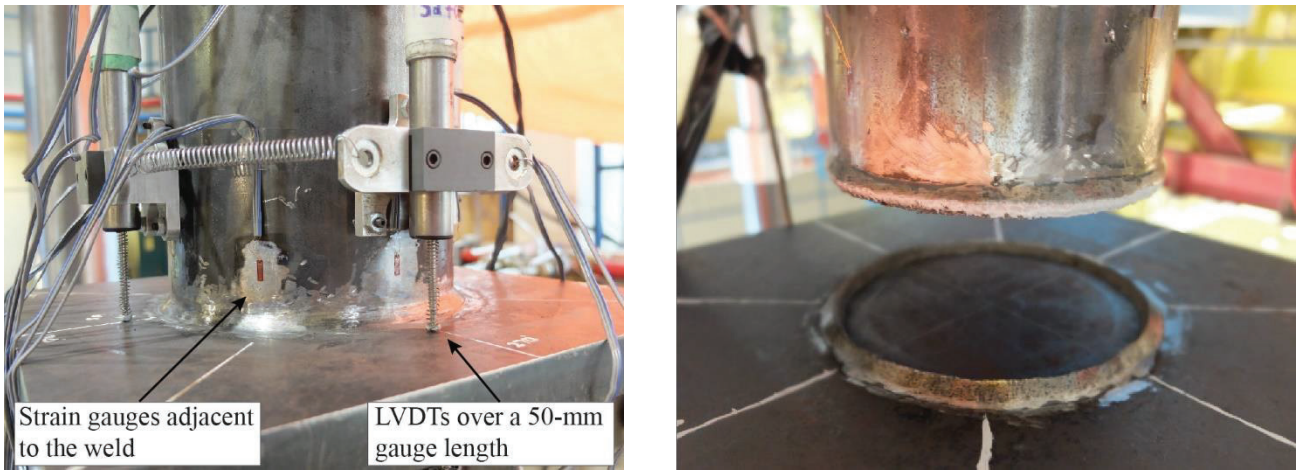

(a) (b)

Fig. 2 CHS-to-rigid plate (a) instrumentation adjacent to the test weld, and (b) typical weld rupture failure mode

3. Fillet welds in CHS-to-rigid plate connections: finite element modelling

The 12 CHS-to-rigid plate experiments were used to validate FE models in ANSYS 14.0 [18]. Unlike the experiments, the models were each comprised of a *single* tension-loaded branch welded to a rigid plate, with nodes restrained on the "underside" of the plate (preliminary FE modelling indicated results were equivalent to modelling the full specimens). Either one quarter or half of the FE connection was modelled using appropriate symmetry boundary conditions depending on the branch angle (θ = 90° or 60°, respectively). A θ = 90° model is shown in Fig. 3. To restrict load transfer to the fillet weld, a 0.25-mm gap was modelled between the CHS and the plate. The size of this gap was selected to minimize its effect on the relationship between l_v, l_h, and t_w. These, and all subsequent FE models, were analyzed under static incremental displacements applied to the branch in the theoretical constant stress region ($3D_b$ from the weld toe).

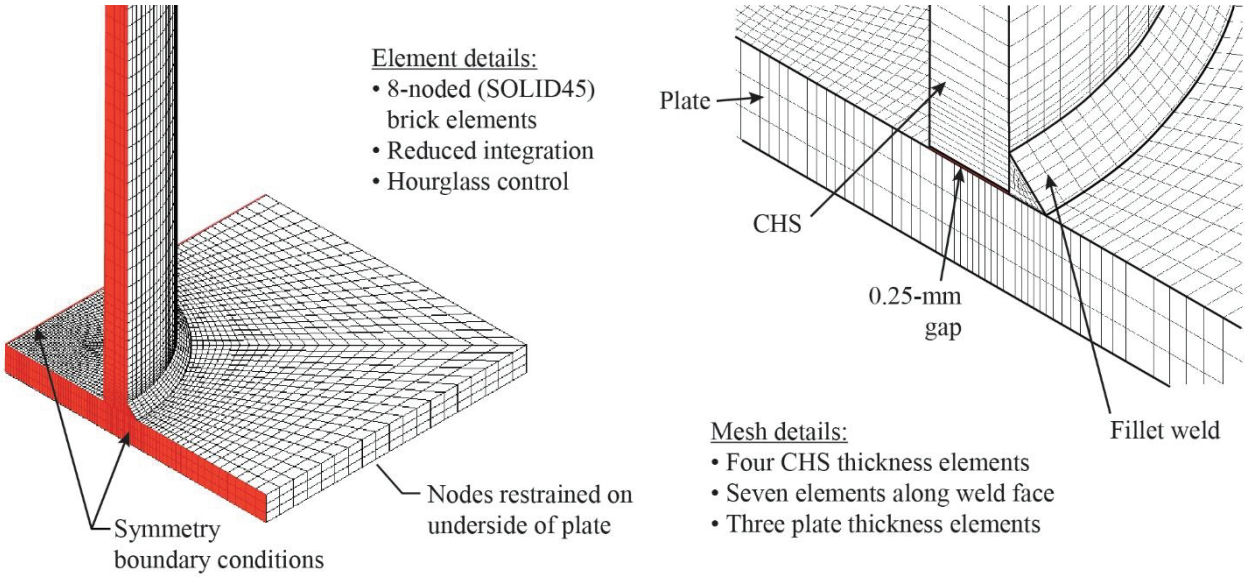

Fig. 3 CHS-to-rigid plate FE model with $\theta = 90°$ and key element and mesh details

3.1. Material modelling

Multi-linear true stress-strain curves for each different material (i.e. the weld metal, plate, and each different branch member) were derived from tensile coupon (TC) tests conducted in accordance with ASTM A370 [14]. Prior to necking, the average engineering stress (σ) and strain (ε) ordinates from the tests were converted to true stress (σ_T) and strain (ε_T) using the following relationships [19]:

$$\sigma_T = \sigma(1+\varepsilon) \tag{2}$$

$$\varepsilon_T = \ln(1+\varepsilon) \tag{3}$$

After necking, an iterative approach based on matching the engineering stress-strain curve of a coupon modelled in ANSYS to that of an experimental test was used to determine ordinates on the σ_T-ε_T curves [20]. The trial-and-error approach involves weighting approximate lower- and upper-bounds to the σ_T-ε_T response. The same elements later employed for the CHS-to-rigid plate models (8-noded brick elements), with large deformations and non-linear material properties, were used. The results of a sensitivity study performed to determine the element type and mesh

arrangement best suited for modelling the full-scale CHS-to-rigid plate connections (i.e. the element and mesh details used) are listed in Fig. 3, shown previously.

3.2. Model fracture criterion

The ANSYS "element death feature" was used to simulate fracture in the fillet welds and/or the plate, which was triggered by a maximum equivalent strain fracture criterion (ε_{ef}) [21, 22].

The maximum equivalent strain fracture criterion (ε_{ef}) was determined by comparing the load-displacement results from six CHS-to-rigid plate FE analyses to corresponding experimental results. By trial and error, the correct value of ε_{ef} for rupture in the weld ($\varepsilon_{ef,weld}$) was determined to be the one that matched the FE and experimental displacement (over the 50-mm gauge length) at weld fracture. Using displacement instead of load to calibrate $\varepsilon_{ef,weld}$ provided more accurate results (in terms of actual-to-predicted fracture loads *and* displacements) because weld rupture typically occurred on the plateau of the load-displacement curve.

The mean value of $\varepsilon_{ef,weld}$ obtained for the six tests was 0.092. This value was used as the criterion to initiate the ANSYS element death feature to reduce the stiffness of an element to nearly zero. The inactive element(s) thereafter sheds load to the surrounding elements (where the equivalent strain, $\varepsilon_e < \varepsilon_{ef}$) and freely deforms. This behaviour is physically comparable to the initiation and propagation of a crack through the weld. An equivalent strain fracture criterion for elements in the plate ($\varepsilon_{ef,plate} = 0.011$) was also calibrated, and determined from five previous tests on RHS-to-rigid plate connections by Frater [23] that failed in this manner (by plate rupture).

3.3. Model validation

The ultimate load predicted by the FE models (P_{FE}) for all 12 CHS-to-rigid plate experiments is shown in Table 2 (presented previously). It can be seen that the models provided good predictions of P_a'. The mean of the ratio of actual-to-predicted ultimate loads in Table 2 (P_a'/P_{FE}) is 1.01, with a coefficient of variation (COV) of 0.10.

The FE load-displacement curves are compared to the experimental curves in Fig. 4 for six (out of the 12) tests. Even though weld penetration was ignored (because it was shown to be minimal for the chosen WPS) and average

values of the weld dimensions (t_w, l_v and l_h) were used, the FE and experimental load-displacement curves show good agreement.

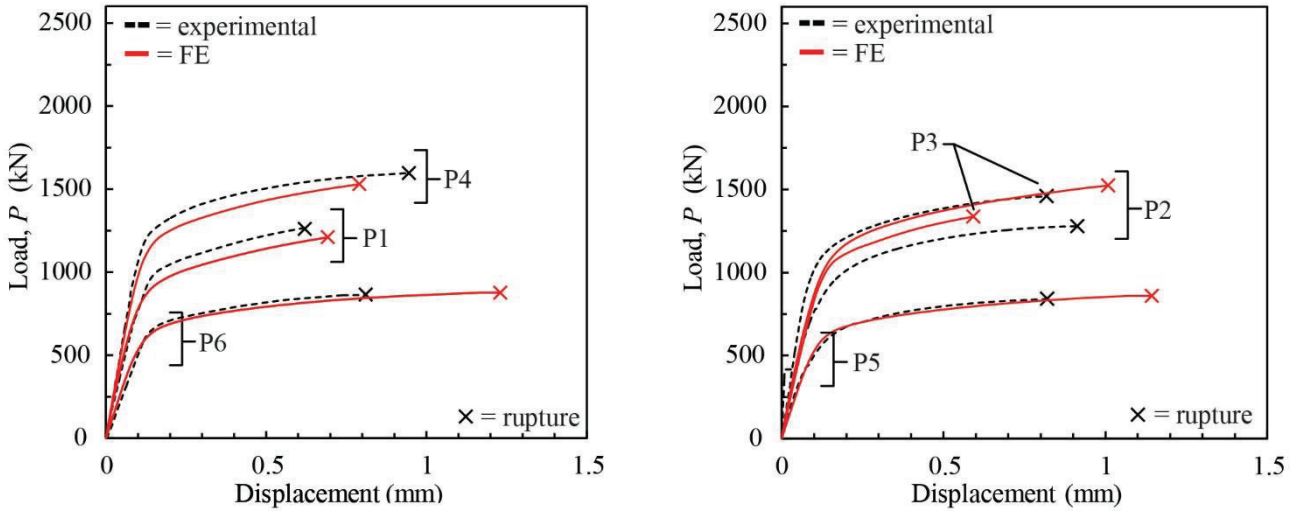

Fig. 4 Comparison of CHS-to-rigid plate FE and experimental load-displacement responses: (a) test nos. P1, P4 and P6; (b) test nos. P2, P3 and P5

3.4. Parametric study

An FE parametric study was thus conducted to extend the database in which the ratio of weld size to branch thickness (t_w/t_b = 0.35, 0.50, 0.71, 0.90, and 1.06) and the CHS branch slenderness (D_b/t_b = 9.1, 12.5, 20, 30, 40, and 50) were varied. For these FE models, θ = 90°; however, four additional FE models (with t_w/t_b = 0.50, D_b/t_b = 12.5 or 50, and θ = 60° or 75°) were later analysed to determine the effect of branch inclination angle on the weld strength. In all models, fillet welds were modelled with equal-sized legs, and the same CHS diameter and plate thickness were used (D_b = 168 mm and t_p = 25 mm). Additionally, the same set of material properties were used (for the weld, the CHS, and the plate). These were taken as the most nominally matched weld and base metal materials from the CHS-to-rigid plate experiments (i.e. test nos. P1, P2, P7, and P8 in Table 1).

3.4.1. Results of the parametric study

Weld rupture occurred in 25 (out of the 30) parametric CHS-to-rigid plate models with $\theta = 90°$. In five of these 25 tests, the branch yielded before the weld ruptured; hence, 20 of these tests were weld-critical. Failure modes, and the non-dimensional average stress on the weld throat at failure (P_{FE}/A_wF_{EXX}, herein called the weld strength), are summarized in Table 3. Table 3 shows that in general the weld strength decreases as both t_w/t_b and D_b/t_b increase.

Table 3. Non-dimensional parameters, P_{FE}/A_wF_{EXX}, and failure mode for CHS-to-rigid plate FE analyses

		t_w/t_b				
t_b mm	D_b/t_b	0.35	0.50	0.71	0.90	1.06
3.36	50	0.85 W	0.87 W	0.81 W	0.76 W	0.73 W †
4.20	40	0.89 W	0.86 W	0.82 W	0.76 W	0.73 W †
5.59	30	0.88 W	0.88 W	0.82 W	0.78 W	0.74 W †
8.40	20	0.90 W	0.88 W	0.85 W	0.80 W †	0.76 W †
13.44	12.5	0.93 W	0.89 W	0.87 W	0.79 P †	0.71 P †
18.48	9.1	0.92 W	0.90 W	0.83 P	0.71 P†	0.65 P †

Note: W = rupture through the weld; P = rupture only in the plate.
† Branch yielded before weld ruptured.

Based on a comparison of the results of the four additional FE models (with $\theta = 60°$ or 75°) to $\theta = 90°$ models with the same values of t_w/t_b and D_b/t_b (Fig. 5), it is shown that while the $(1.0+0.5\sin^{1.5}\theta)$ factor predicts a reduction in weld strength as the average loading angle of the weld θ goes from 90° to 60°, this is not the case for CHS-to-rigid plate connections. The forthcoming reliability analysis is therefore concerned with applicability of the $(1.0+0.5\sin^{1.5}\theta)$ factor only to CHS-to-rigid plate connections with $\theta = 90°$, since the above evidence suggests it does not predict the correct trend when θ is less than 90°.

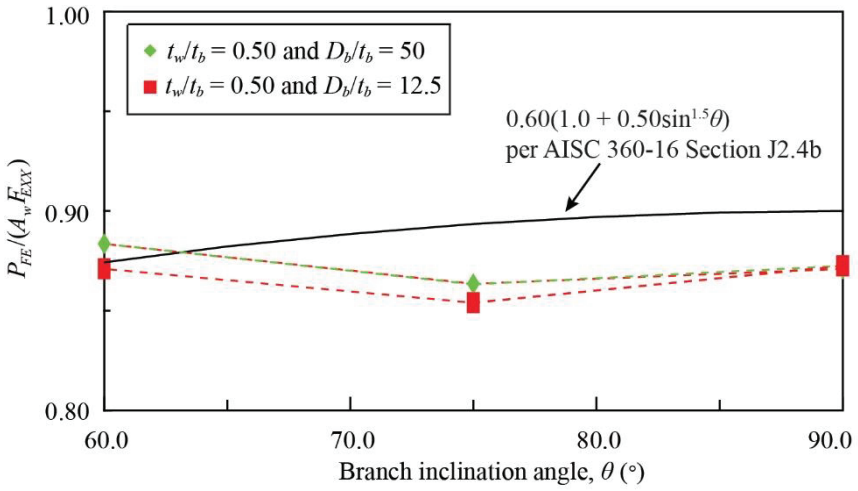

Fig. 5 Effect of branch inclination angle on fillet weld strength in CHS-to-rigid plate connections

4. Evaluation of the (1.0+0.5sin$^{1.5}\theta$) factor for fillet welds to CHS branches

4.1. Existing AISC 360-16 provisions for design of fillet welds to CHS branches

According to AISC 360-16 Section J2.4a, the nominal strength of a fillet weld (P_n) is based on the limit state of shear rupture along the plane of the weld effective throat in accordance with Eq. (4):

$$P_n = 0.60 F_{EXX} A_w \tag{4}$$

where A_w = the effective weld throat area (= $t_w l_w$).

An LRFD resistance factor for fillet welds, ϕ, equal to 0.75, is then applied to determine the design (available) strength.

For parallel weld elements with a uniform leg size, loaded through the centre of gravity, AISC 360-16 Section J2.4b permits the use of the (1.0+0.5sin$^{1.5}\theta$) factor when determining P_n. Thus:

$$P_n = 0.60(1.0 + 0.50\sin^{1.5}\theta) F_{EXX} A_w \tag{5}$$

where θ = angle of loading measured from the weld longitudinal axis (in degrees).

Either Eq. (4) or (5) could be used to design fillet welds around the perimeter of a CHS welded to a rigid plate.

4.2. Safety level inherent in AISC 360-16 fillet weld design provisions

To assess whether adequate safety margins are inherent in the $(1.0+0.5\sin^{1.5}\theta)$ factor for fillet welds in CHS-to-rigid plate connections, the structural reliability (or safety index) (β^+) can be calculated, and compared to the target value of 4.0 (per Section B3.1 of the AISC 360-16 Commentary), using a simplified reliability analysis in which the resistance factor, ϕ, is given by Eq. (6) [24, 25]:

$$\phi = \phi_{\beta+}\rho_R e^{-\alpha_R \beta^+ V_R} \tag{6}$$

where α_R = coefficient of separation taken as 0.55 [24]; ρ_R = bias coefficient for resistance (mean ratio of actual-to-predicted weld strength); V_R = associated coefficient of variation (COV) of ρ_R; and $\phi_{\beta+}$ = adjustment factor for β^+ that is needed when $\beta^+ \neq 3.0$ [25]. A formula for $\phi_{\beta+}$ was derived by Franchuk et al. [26]:

$$\phi_{\beta+} = 0.0062(\beta^+)^2 - 0.131\beta^+ + 1.338 \tag{7}$$

The mean actual-to-predicted weld strength ratio (ρ_R) was taken as the average over all of the $\theta = 90°$ weld-critical tests of P_a' (or P_{FE}) divided by P_n, with P_n calculated using Eq. (5), and the measured values of A_w and F_{EXX}. The reliability analysis parameters, and the results of the reliability analysis, are shown in Table 4. The implied safety index, β^+, = 3.69 < 4.0 for Eq. (5). This indicates that the AISC 360-16 Section J2.4b formula is unsafe for fillet welds to CHS branches when the welds are fully effective. Fig. 6a shows the correlation of the existing AISC 360-16 predicted nominal strengths using Eq. (5) with the FE and experimental results.

Table 4. AISC 360-16 reliability analysis parameters (CHS-to-rigid plate experiments and FE analyses)

	Section J2.4b $P_n = 0.60(1.0+0.50\sin^{1.5}\theta)F_{EXX}A_w$	Section J2.4a $P_n = 0.60F_{EXX}A_w$
number of tests	26	26
ϕ	0.75	0.75
ρ_R	0.94	1.41
V_R	0.08	0.08
ϕ_{β^+}	0.94	0.72
β^+	3.69 < 4.0	7.01 ≥ 4.0

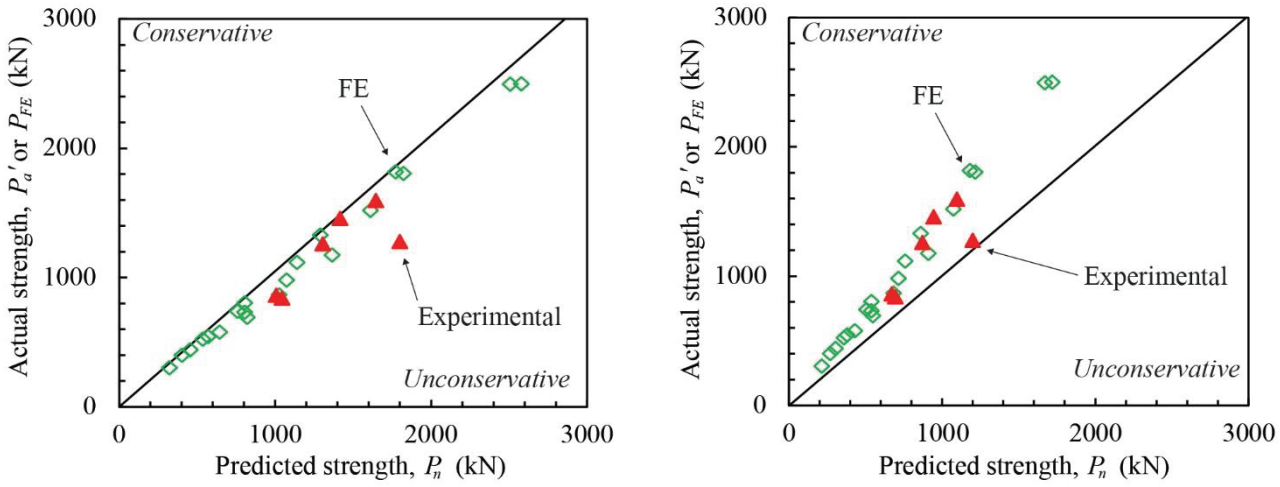

Fig. 6 Correlation of AISC 360-16 fillet weld design provisions with 26 weld-critical $\theta = 90°$ CHS-to-rigid plate test results: (a) Section J2.4b [with the $(1.0+0.5\sin^{1.5}\theta)$ factor]; (b) Section J2.4a [without the $(1.0+0.5\sin^{1.5}\theta)$ factor]

If the reliability analysis is repeated with P_n calculated using Eq. (4) [i.e. omitting the $(1.0+0.5\sin^{1.5}\theta)$ factor], the correlation in Fig. 6b results, and the implied safety index, $\beta^+ = 7.01 > 4.0$ (Table 4). It can therefore be concluded that, for fillet-welded CHS-to-rigid plate connections in which the welds are fully effective, the provisions of AISC 360-16 Section J2.4b should not be used. It follows that the $(1.0+0.5\sin^{1.5}\theta)$ factor should also not be used with CHS branches when fillet welds are partially effective, such as in CHS-to-CHS connections.

5. Fillet welds in CHS-to-CHS X-connections: experiments

5.1. Mechanical and geometrical properties

Six CHS-to-CHS X-connections, comprising 12 weld-critical experiments (two per connection), were designed and fabricated from ASTM A500 [13] dual-certified Grade B/C cold-formed CHS, and fillet welded using the same FCAW process used for the CHS-to-rigid plate connections. The CHS members were selected to cover a wide range of branch-to-chord diameter ratios ($\beta = D_b/D$), chord wall slenderness values (D/t), and branch inclination angles (θ) (Table 5), within Ψ limits for fillet welds to develop the full throat thickness without Z-loss ($60° < \Psi < 120°$, according to AWS D1.1-15). Branches were a minimum length (l_b) of $6D_b$ to avoid shear lag effects at the connection [17], and profiled to saddle perfectly onto the chords, without edge bevelling. The chords were a minimum length (l) to avoid end effects at the connection [27], and left uncapped.

Table 5. Measured geometric properties and ultimate loads (experimental and FE) for $\theta = 90°$ and $\theta = 60°$ CHS-to-CHS X-connection experiments

Test no.	CHS branch	CHS chord		Average weld dimensions							
	$D_b \times t_b$	$D \times t$	θ	l_w	t_w	l_v	l_h	P_a	P_a'	P_{FE}	P_a'/P_{FE}
	mm × mm	mm × mm	°	mm	mm	mm	mm	kN	kN	kN	
X1	102.0 × 7.34	273.5 × 11.69	90	322	4.08	6.86	6.17	672	672	655	1.03
X2	102.0 × 7.34	273.5 × 11.69		322	4.37	7.23	6.65	678	678	690	0.98
X3	102.0 × 7.34	406.5 × 12.34		320	3.56	5.16	5.78	608	608	543	1.12
X4	102.0 × 7.34	406.5 × 12.34		320	3.14	4.54	5.08	540	540	495	1.09
X5	127.4 × 11.55	273.5 × 11.69		406	3.63	5.94	5.93	653	653	762	0.86
X6	127.4 × 11.55	273.5 × 11.69		406	4.00	7.05	6.06	609	653	811	0.80
X7	127.4 × 11.55	406.5 × 12.34		403	3.16	4.83	5.03	557	557	631	0.88
X8	127.4 × 11.55	406.5 × 12.34		403	3.47	5.60	5.19	556	557	617	0.90
X9	102.0 × 7.34	410.0 × 12.21	60	345	3.58	5.83	5.59	721	721	640	1.13
X10	102.0 × 7.34	410.0 × 12.21		345	3.79	6.29	5.83	538	721	672	1.07
X11	127.4 × 11.55	410.0 × 12.21		434	3.95	5.68	8.01	761	761	903	0.84
X12	127.4 × 11.55	410.0 × 12.21		434	3.38	5.39	6.00	798	850	798	1.06

Note: P_a = actual (experimental) load at weld rupture; P_a' = greatest actual (experimental) load sustained by the weld; P_{FE} = failure load in the finite element model.

Welds were again ground flat, and components of l_v and l_h parallel to the branch axis were measured at 12 or 15 different locations along the weld length (for branches with D_b = 102.0 or 127.4 mm, respectively). These measurements were used to model the 3D weld around the entire joint in Solidworks, with actual measured values of D_b and D. Sections were then cut through the weld (in Solidworks), in the plane of Ψ (i.e. the plane normal to the weld throat dimensions) so that the correct values of l_v, l_h and t_w could be measured (Fig. 7). The total weld length (l_w), and the weld length tributary to each cut through the weld, were calculated by modifying Luyties & Post's [16]

method for calculating Ψ to give a near-perfect solution for the distance between points along the weld length (and then summing up these distances). The weld area (A_w) was hence taken as the sum of: (t_w × tributary weld length) around the entire joint.

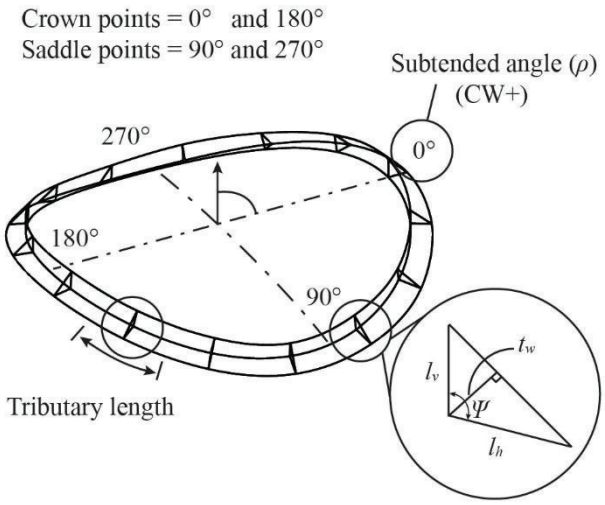

Fig. 7 3D weld and section cuts (in Solidworks)

The average yield stress (F_y) and ultimate stress (F_u, or F_{EXX} for the weld metal) of the CHS branches, chord, and weld metal, determined by tensile coupon testing in accordance with ASTM A370 [14] or AWS D1.1 [15] (for the weld metal), are summarized in Table 6.

Table 6. Measured material properties for the 12 CHS-to-CHS X-connection experiments

	CHS branch		CHS chord		Weld metal	
Test No.	F_y MPa	F_u MPa	F_y MPa	F_u MPa	F_y MPa	F_{EXX} MPa
X1 and X2	373	454	460	540	517	577
X3 and X4	373	454	355	464	517	577
X5 and X6	431	488	460	540	517	577
X7 and X8	431	488	355	464	517	577
X9 and X10	373	454	373	485	517	577
X11 and X12	431	488	373	485	517	577

5.2. Test set-up and instrumentation

Quasi-static axial tension was applied to the end of each branch on either side of the connection, and hence to the weld, by the same MTS UTM used previously for the CHS-to-plate tests. The testing arrangement, shown in Fig. 8a, consisted of the following instrumentation:

(a) four linear strain gauges (SGs) equally spaced around the perimeter of one branch, at mid length, which confirmed uniform tensile loading of the branch;

(b) seven additional SGs with the same orientation, 20 mm away from the weld toe around half the weld perimeter (i.e. on one side of the branch only, due to symmetry) that monitored non-uniform loading of the weld (Fig. 8b); and

(c) an LED scanner, with three LED targets (one on each branch, 50 mm above the crown, and one at the connection work point on the chord face parallel to the plane of the connection) that monitored chord deformation (δ) throughout each test (see Fig. 8a).

The value of δ, which is the outward displacement (normal to the chord) of a single branch from the chord centreline [28], was taken as half of the vertical displacement between the LEDs on each branch. It therefore represents the average deformation on both sides of the connection.

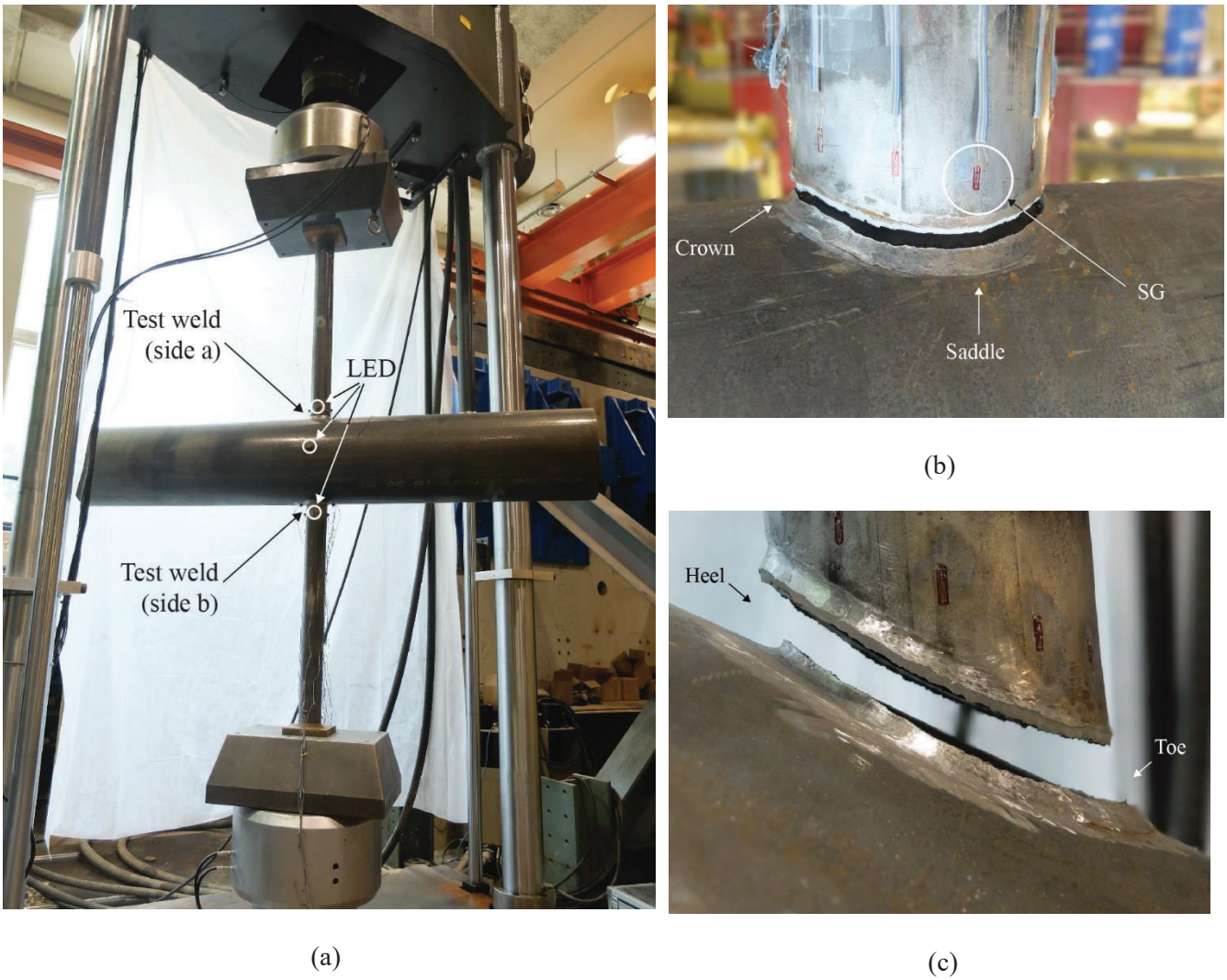

(a) (b) (c)

Fig. 8 CHS-to-CHS X-connection experiments: (a) testing arrangement; (b) weld fracture in test no. X5 (θ = 90°); and (c) weld fracture in test no. X9 (θ = 60°)

The procedure used for the CHS-to-plate tests to rupture both welds in the connection was again used for the CHS-to-CHS tests. All 12 test joints failed by weld rupture along a plane through the weld (Fig. 8b,c). The weld ultimate loads (P_a' in Table 5) were measured using a load cell in-line with the UTM actuator, and taken as the greatest load sustained by the weld (even if weld rupture occurred at a lower load during a later loading). The column P_a in Table 5 gives the actual load at weld rupture.

5.3. Results

Representative graphs of the strain distribution around the branch adjacent to the test weld, for various levels of applied load, are given in Fig. 9. For $\theta = 90°$ connections (Fig. 9a), the tensile strain (and hence tensile load) peaks at the saddle point ($\rho = 90°$). Demand on the weld is smallest at the crown points ($\rho = 0°$ and 180°); much of the weld even remained in compression for the majority of the tests. This phenomenon equates to a non-uniform loading of the weld perimeter, and indicates that weld effective lengths are present in CHS-to-CHS connections.

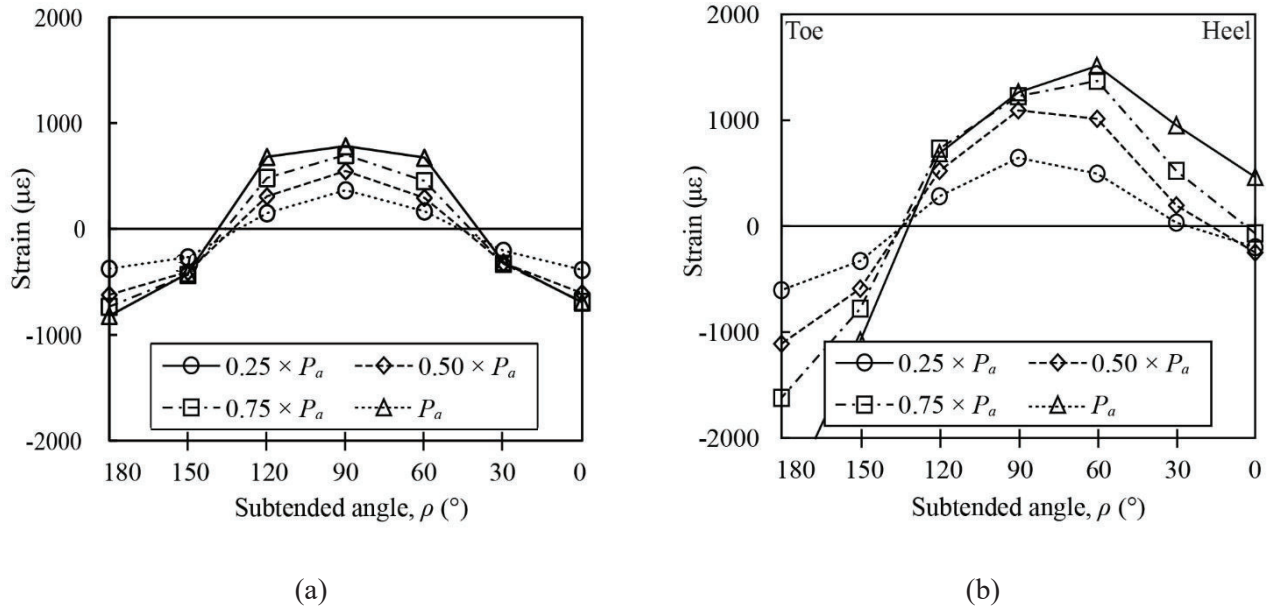

(a) (b)

Fig. 9 Typical strain distributions adjacent to test welds: (a) test no. X7 ($\theta = 90°$), (b) test no. X9 ($\theta = 60°$)

For $\theta = 60°$ connections, the peak tensile strain is initially at the saddle point ($\rho = 90°$) (Fig. 9b), but moves towards the heel as the load increases. This may be due to secondary bending effects from connection flexibility and joint rotation which do not exist in real structures when the chord ends are prevented from moving because they are connected to other members.

6. Fillet welds in CHS-to-CHS X-connections: finite element modelling

CHS-to-CHS X-connection FE models were hence developed to replicate the experimental tests and extend the test database. The models were developed using the same approach as the CHS-to-rigid plate connections, including

use of a 0.25-mm gap between the branches and the chord. Although it was possible to model just one eighth of the non-inclined ($\theta = 90°$) connections due to symmetry about three principal planes passing through the work point, one half of every connection was modelled instead to accommodate the inclined branch ($\theta < 90°$) cases. The element and mesh details used were the same as those for the CHS-to-plate FE tests; these are depicted in Fig. 10, and were shown to be suitable by conducting a separate sensitivity study.

An FE fracture criterion for the weld ($\varepsilon_{ef,weld} = 0.32$) was applied to only one weld in the connection (i.e. the "critical weld" in Fig. 10). The difference in $\varepsilon_{ef,weld}$ between the CHS-to-CHS X-connections ($\varepsilon_{ef,weld} = 0.32$) and the CHS-to-rigid plate connections ($\varepsilon_{ef,weld} = 0.092$) is due to different triaxiality at the location of rupture [21, 29], and is expected. Base metal rupture was not observed in any tests, and was hence not included in the model.

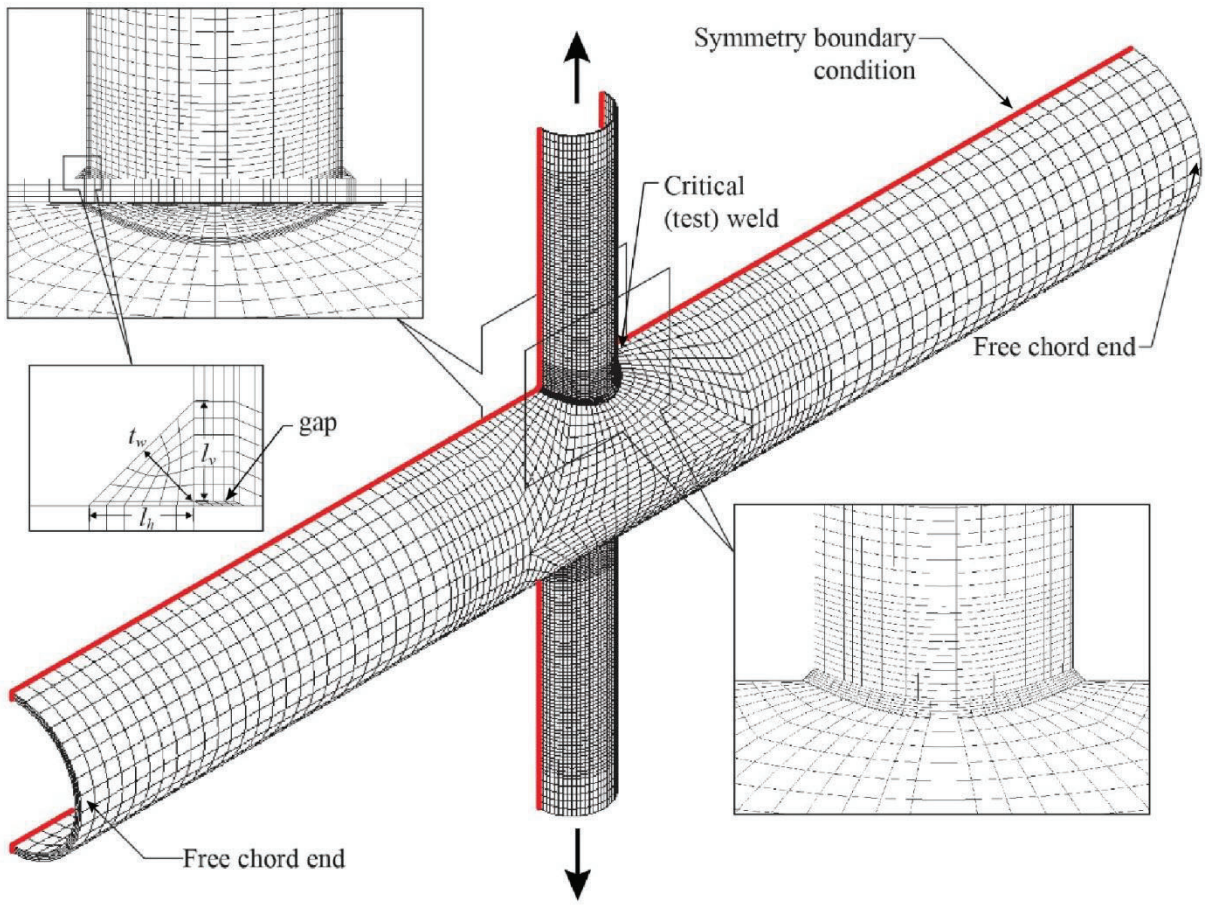

Fig. 10 CHS-to-CHS FE model with $\theta = 90°$

6.1. Model validation

Fig. 11a,b compares the experimental and FE load-deformation curves for six (of the 12) specimens. The deformations have been normalized, by dividing by D, so that curves for connections with different chord diameters can be compared on the same plot. For clarity, the six curves have been divided between two graphs. Despite the same assumptions made for the CHS-to-plate FE models (weld penetration was ignored and average values of the weld dimensions were used), the FE and experimental load-displacement curves show good agreement. In Table 5 (shown previously) the mean actual-to-FE predicted ultimate load (P_a'/P_{FE}) is 0.98, with a coefficient of variation (COV) of 0.12. These values indicate that the model made acceptable predictions of P_a' across all tests.

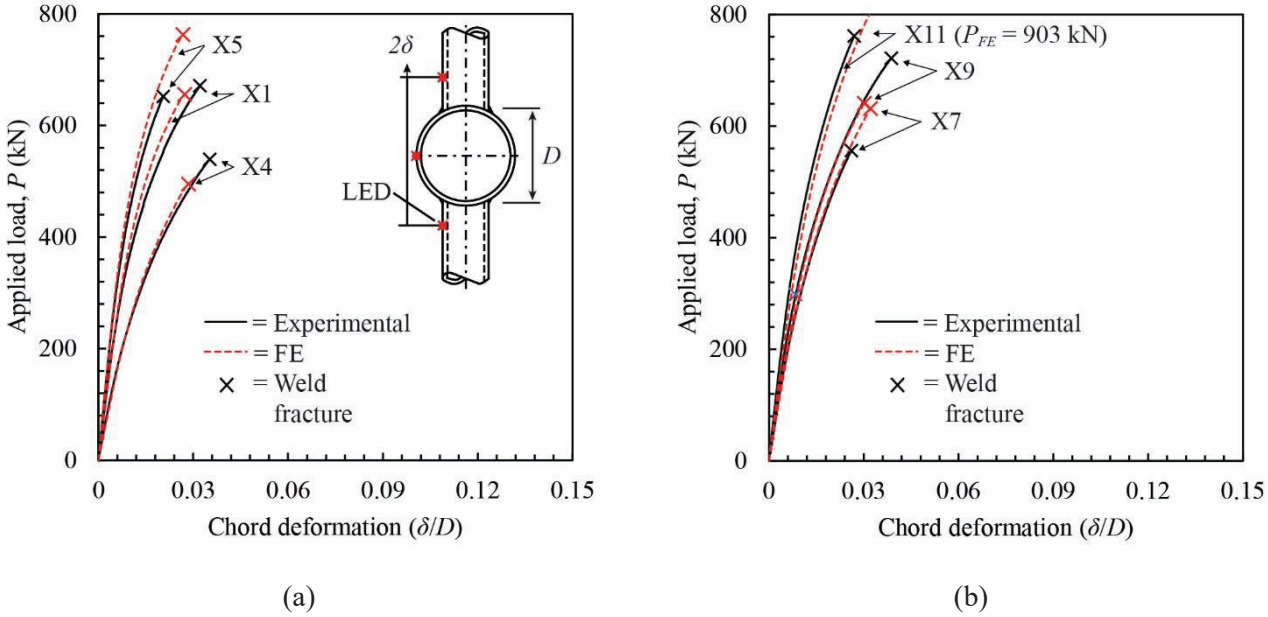

Fig. 11 Comparison of CHS-to-CHS FE and experimental load-displacement responses: (a) test nos. X1, X4 and X5; (b) test nos. X7, X9 and X11

6.2. Parametric study

A range of non-dimensional connection parameters was chosen to cover all permissible fillet-welded connections subject to the following restrictions: (a) the local dihedral angle (Ψ) limits imposed by AWS D1.1-15 Fig. 9.10 and Table 9.5 ($60° \leq \Psi \leq 120°$); (b) the limits of applicability of connection design formulae in AISC 360-16 Table K3.1, which are given in AISC 360-16 Table K3.1A; and (c) the range of standard CHS sections available

for designers in Table 1-13 of the *Steel Construction Manual* [30]. The parameters varied were: the branch inclination angle (θ = 60°, 70°, 80°, and 90°); the chord slenderness (D/t = 10, 20, 30, 40, and 50); the branch-to-chord diameter ratio (β = 0.10, 0.20, 0.30, 0.40, and 0.50); and the branch-to-chord thickness ratio (τ = 0.20, 0.40, 0.60, 0.80, and 1.00). Although a total of 500 permutations exist for the values given, there are several practical limitations that must be considered. First, available CHS sections limit branch slenderness ratios (D_b/t_b) to between about 10 and 50. Secondly, not all combinations of β and θ produce Ψ between 60° and 120° (to qualify as a fillet weld) along the entire weld length. A comprehensive parametric study was hence performed by modelling β up to 0.30 for 60° connections and β up to 0.50 for all other branch angles. A total of 256 CHS-to-CHS X-connection models was thus analysed.

6.2.1. Details of the parametric models

The CHS-to-CHS X-connection parametric FE models had constant branch diameters (D_b) of 200 mm and $t_w = 0.50t_b$ to ensure that the branch yield capacity was not reached before weld fracture. As in the experiments, the ends of the chords were uncapped. The length of the chord (l) was $10D$ (when $D/t > 25$) or $6D$ (when $D/t \leq 25$) to prevent chord end effects at the connection (i.e. the effect of the chord end conditions – fixed, pinned, or free, capped or uncapped – on the connection load-displacement response) [27]. The length of the branches (l_b) was $3D_b$, and load was applied to their ends in the theoretical constant stress region [17]. All models used the same set of material properties (for the weld, the branches, and the chord) taken as the most nominally matched weld and base metals from the CHS-to-CHS experiments in Table 6 (i.e. test nos. X5 and X6).

6.2.2. Results of the parametric study

All 256 FE analyses failed by weld fracture while the branches of the connection remained elastic. Fracture initiated in the weld at the saddle point and propagated away from the saddle towards the crown before the maximum load was reached. It was found from these 256 analyses that the weld strength (P_{FE}/A_wF_{EXX}) decreases as D/t, β and τ increase. The branch inclination angle was found to have no significant effect.

7. Evaluation of AISC 360-16 fillet weld design provisions for CHS-to-CHS X-connections

The previous reliability analysis was repeated using all 268 experimental and FE CHS-to-CHS X-connection results to determine the implied safety index, β^+, for the current AISC 360-16 provisions *without* weld effective lengths (i.e. using Section J2.4a). The mean actual-to-predicted weld strength ratio (ρ_R) was hence taken as the average over all tests of P_a' (or P_{FE}) divided by P_n, with P_n calculated using Eq. (4), and the measured values of A_w and F_{EXX}. The analysis determined that $\beta^+ = 4.53 \geq 4.0$ for AISC 360-16 without weld effective lengths. Table 7 summarizes the reliability analysis parameters. A correlation plot is presented in Fig. 12.

Table 7. AISC 360-16 reliability analysis parameters (CHS-to-CHS experiments and FE analyses)

	Section J2.4a $P_n = 0.60F_{EXX}A_w$
number of tests	268
ϕ	0.75
ρ_R	1.38
V_R	0.19
ϕ_{β^+}	0.87
β^+	$4.53 \geq 4.0$

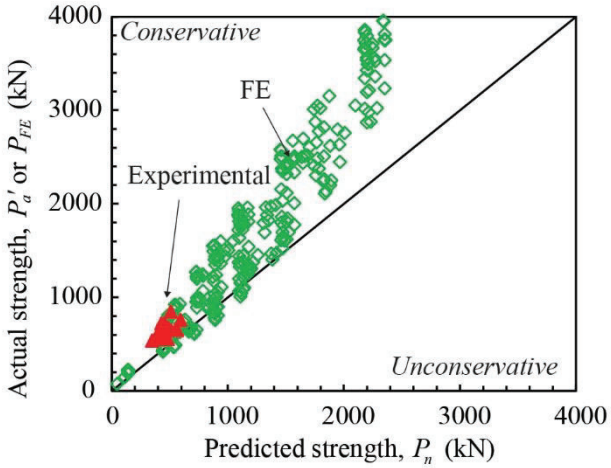

Fig. 12 Correlation of AISC 360-16 Section J2.4a fillet weld design provisions with 268 weld-critical CHS-to-CHS test results

It can therefore be concluded that weld effective lengths are not required for fillet-welded CHS-to-CHS X-connections in conjunction with the AISC 360-16 Section J2.4 code design method, provided that the $(1.0+0.50\sin^{1.5}\theta)$ factor (given in Section J2.4b) is not used.

8. Conclusions and recommendations

Based on 12 experiments and 34 FE analyses on fillet-welded CHS-to-rigid plate connections, it was shown that the $(1.0+0.5\sin^{1.5}\theta)$ factor in AISC 360-16 Section J2.4b fails to provide an adequate reliability (safety) index ($\beta^+ = 3.69 < 4.0$) for fillet welds around CHS branches.

Based on 12 further experiments and 256 further FE analyses on fillet-welded CHS-to-CHS X-connections, it was shown that the current AISC 360-16 Section J2.4 specification provisions for fillet welds provide adequate structural reliability ($\beta^+ = 4.53 \geq 4.0$) without weld effective lengths (i.e. when the total weld length is used to determine the weld strength), provided that the $(1.0+0.50\sin^{1.5}\theta)$ factor is not used. This is because the analysis method of AISC 360-16 Section J2.4 considers the axial force in the branch member to be resisted only by shear stress on the weld throat, which is a conservative assumption.

It is therefore recommended that the provisions of AISC 360-16 Section J2.4 be used without the $(1.0+0.50\sin^{1.5}\theta)$ factor [i.e. taking $\theta = 0°$ in the term $(1.0+0.50\sin^{1.5}\theta)$] for *all* fillet welds around the perimeter of CHS branches (including CHS-to-CHS connections, where weld effective lengths are theoretically present, and CHS connections in which the welds are fully effective, e.g. CHS-to-rigid plate connections). Furthermore, it is recommended that AISC advocate 100% weld effective lengths for fillet-welded CHS-to-CHS X-connections, subject to the above restriction on the $(1.0+0.50\sin^{1.5}\theta)$ factor.

Acknowledgements

The authors would like to acknowledge the laboratory contributions of Ms. J. Lu and Mr. F. Wei (summer research students) to this work. Hollow structural sections for this project were donated by Atlas Tube, Harrow, Ontario, and fabrication services were donated by Walters Inc., Hamilton, Ontario. The financial support of the Natural Sciences and Engineering Research Council of Canada (NSERC) is greatly appreciated.

Symbols

A_w	effective throat area of weld (= $t_w l_w$)
D	overall diameter of the CHS chord
D_b	overall diameter of the CHS branch
F_{EXX}	electrode ultimate strength
F_u	ultimate stress of the CHS; ultimate stress of the plate
F_y	yield stress of the CHS; yield stress of the plate
P	applied force
P_{FE}	failure load in the finite element model
P_a	actual (experimental) load at weld rupture
P_a'	greatest actual (experimental) load sustained by the weld
P_n	nominal/predicted weld fracture load
V_R	coefficient of variation of ρ_R
Z	weld throat dimension when full root penetration is achieved
l	length of the CHS chord member
l_b	length of the CHS branch member
l_h	weld leg measured along the plate; weld leg measured along the CHS chord
l_v	weld leg measured along the CHS branch
l_w	total weld length
t	wall thickness of the CHS chord member
t_b	wall thickness of the CHS branch member
t_p	plate thickness
t_w	weld effective throat dimension
α_R	coefficient of separation (taken to be 0.55)
β	ratio of overall branch diameter to chord diameter
β^+	safety index
δ	chord deformation

ε	engineering strain
ε_T	true strain
ε_e	equivalent (von Mises) strain
ε_{ef}	equivalent (von Mises) strain at rupture for failure criterion
$\varepsilon_{ef,plate}$	equivalent (von Mises) strain at rupture for plate failure criterion
$\varepsilon_{ef,weld}$	equivalent (von Mises) strain at rupture for weld failure criterion
θ	branch inclination angle; angle of loading measured from the weld longitudinal axis for fillet weld strength calculation (in degrees)
ρ	subtended angle around the branch, measured from heel
ρ_R	bias coefficient for the resistance
σ	engineering stress
σ_T	true stress
τ	branch-to-chord thickness ratio
ϕ	resistance factor (associated with the LRFD method)
ϕ_{β^+}	adjustment factor for β^+
Ψ	local dihedral angle (angle between the base metal fusion faces)

References

[1] ISO. (2013). ISO 14346:2013 (E). Static design procedure for welded hollow section joints – Recommendations. Geneva, Switzerland.

[2] Frater, G. S. & Packer, J. A. (1992a). Weldment design for RHS truss connections. I: Applications. Journal of Structural Engineering, American Society of Civil Engineers 118(10): 2784-2803.

[3] Frater, G. S. & Packer, J. A. (1992b). Weldment design for RHS truss connections. II: Experimentation. Journal of Structural Engineering, American Society of Civil Engineers 118(10): 2804-2820.

[4] Packer, J. A. & Cassidy, C. E. (1995). Effective weld length for HSS T, Y, and X connections. Journal of Structural Engineering, American Society of Civil Engineers 121(10): 1402-1408.

[5] McFadden, M. R. & Packer, J. A. (2014). Effective weld properties for hollow structural section T-connections under branch in-plane bending. Engineering Journal, American Institute of Steel Construction 51(4): 247-266.

[6] Tousignant, K. & Packer, J. A. (2015). Weld effective lengths for rectangular HSS overlapped K-connections. Engineering Journal, American Institute of Steel Construction 52 (4): 259-282.

[7] AISC. (2016). ANSI/AISC 360-16. Specification for structural steel buildings. Chicago, IL, USA.

[8] Packer, J. A. & Sun, M. (2011). Weld design for rectangular HSS connections. Engineering Journal, American Institute of Steel Construction 48(1): 31-48.

[9] McFadden, M. R. & Packer, J. A. (2013). Effective weld properties for RHS-to-RHS moment T-connections. Phase 1 Report to the American Institute of Steel Construction. Toronto, Canada: University of Toronto.

[10] McFadden, M. R., Sun, M. & Packer, J. A. (2013). Weld design and fabrication for RHS connections. Steel Construction – Design and Research 6(1): 5-10.

[11] AISC. (2010). ANSI/AISC 360-10. Specification for structural steel buildings. Chicago, IL, USA.

[12] Marshall, P.W. (1992). Design of welded tubular connections – Basis and use of AWS code provisions. Amsterdam, The Netherlands: Elsevier.

[13] ASTM. (2018). ASTM A500/A500M-18. Standard specification for cold-formed welded and seamless carbon steel structural tubing in rounds and shapes. West Conshohocken, PA, USA.

[14] ASTM. (2017). ASTM A370-17a. Standard test methods and definitions for mechanical testing of steel products. West Conshohocken, PA, USA.

[15] AWS. (2015). AWS D1.1/D1.1M:2015. Structural welding code – Steel, 23rd ed., Miami, FL, USA.

[16] Luyties, W. H. & Post, J. W. (1988). Local dihedral angle equations for tubular joints and related applications. Welding Journal, American Welding Society 77(4): 51-60.

[17] Mehrotra, B. L. & Govil, A. K. (1972). Shear lag analysis of rectangular full-width tube connections. Journal of the Structural Division, American Society of Civil Engineers 98(ST1): 287-305.

[18] Swanson Analysis Systems. (2011). ANSYS ver. 14.0. Houston, TX, USA.

[19] Boresi, A. P. & Schmidt, R.J. (2003). Advanced mechanics of materials, 6th ed. NJ, USA: John Wiley and Sons, Inc.

[20] Ling, Y. (1996). Uniaxial true stress-strain after necking. AMP Journal of Technology 5(1): 37-48.

[21] Voth, A. P. & Packer, J. A. (2012). Branch plate-to-circular hollow structural section connections. I: Experimental investigation and finite-element modeling. Journal of Structural Engineering, American Society of Civil Engineers 138(8): 995-1006.

[22] Martinez-Saucedo, G., Packer, J. A. & Willibald, S. (2006). Parametric finite element study of slotted end connections to circular hollow sections. Engineering Structures 28(14): 1956-1971.

[23] Frater, G. S. (1986). Weldment design for hollow structural section joints. M.A.Sc. thesis. Toronto, Canada: University of Toronto.

[24] Ravindra, M. K. & Galambos, T. V. (1978). Load and resistance factor design for steel. Journal of the Structural Division. American Society of Civil Engineers 104(9): 1337-1353.

[25] Fisher, J. W., Galambos, T. V., Kulak, G. L. & Ravindra, M. K. (1978). Load and resistance factor design criteria for connectors. Journal of the Structural Division, American Society of Civil Engineers 104(9): 1427-1441.

[26] Franchuk, C. R., Driver, R. G. & Grondin, G. Y. (2002). Block shear failure of coped steel beams. Proc. Annual Conf. of the Canadian Society for Civil Engineering, Montreal, 5-8 June 2002. 1000-1009.

[27] van der Vegte, G. J. & Makino, Y. (2010). Further research on chord length and boundary conditions of CHS T- and X-joints. Advanced Steel Construction 6(3): 879-890.

[28] Packer, J. A., Choo, Y. S., Shen, W., Wardenier, J., van der Vegte, G. J., & Mustard, T. (2012). CIDECT Report 5BW-2/12. Axially loaded T and X joints of elliptical hollow sections. Geneva, Switzerland: CIDECT.

[29] Kanvinde, A. M. & Deierlein, G. G. (2006). Void growth model and stress modified critical strain model to predict ductile fracture in structural steels. Journal of Structural Engineering, American Society of Civil Engineers 132(12): 1907-1918.

[30] AISC. (2017). Steel construction manual, 15th ed., Chicago, IL, USA.

Figure Captions

Fig. 1 Experimental test specimens: (a) CHS-to-rigid plate connection; (b) CHS-to-CHS X-connection

Fig. 2 CHS-to-rigid plate (a) instrumentation adjacent to the test weld, and (b) typical weld rupture failure mode

Fig. 3 CHS-to-rigid plate FE model with $\theta = 90°$ and key element and mesh details

Fig. 4 Comparison of CHS-to-rigid plate FE and experimental load-displacement responses: (a) test nos. P1, P4 and P6; (b) test nos. P2, P3 and P5

Fig. 5 Effect of branch inclination angle on fillet weld strength in CHS-to-rigid plate connections

Fig. 6 Correlation of AISC 360-16 fillet weld design provisions with 26 weld-critical $\theta = 90°$ CHS-to-rigid plate test results: (a) Section J2.4b [with the $(1.0+0.5\sin^{1.5}\theta)$ factor]; (b) Section J2.4a [without the $(1.0+0.5\sin^{1.5}\theta)$ factor]

Fig. 7 3D weld and section cuts (in Solidworks)

Fig. 8 CHS-to-CHS X-connection experiments: (a) testing arrangement; (b) weld fracture in test no. X5 ($\theta = 90°$); and (c) weld fracture in test no. X9 ($\theta = 60°$)

Fig. 9 Typical strain distributions adjacent to test welds: (a) test no. X7 ($\theta = 90°$), (b) test no. X9 ($\theta = 60°$)

Fig. 10 CHS-to-CHS FE model with $\theta = 90°$

Fig. 11 Comparison of CHS-to-CHS FE and experimental load-displacement responses: (a) test nos. X1, X4 and X5; (b) test nos. X7, X9 and X11

Fig. 12 Correlation of AISC 360-16 Section J2.4a fillet weld design provisions with 268 weld-critical CHS-to-CHS test results

Fillet welds around circular hollow sections

Kyle Tousignant[a*] and Jeffrey A. Packer[b]

[a] Department of Civil and Resource Engineering, Dalhousie University, Sexton Campus, 1360 Barrington Street, Halifax, NS, B3H 4R2, Canada

[b] Department of Civil & Mineral Engineering, University of Toronto, 35 St. George Street, Toronto, ON, M5S 1A4, Canada

[*] Corresponding Author. E-mail: kyle.tousignant@dal.ca; Tel: +1-902-494-3080; ORCID: 0000-0001-5975-7532

Abstract

An experimental and numerical research program was conducted to evaluate the safety of North American design rules for fillet welds around the perimeter of steel circular hollow sections (CHS). This assessment was performed in the context of the current American Institute of Steel Construction (AISC) steel building specification, AISC 360. Specifically, the appropriateness of the fillet weld directional strength-enhancement factor in AISC 360-16 Clause J2.4b was investigated for fillet welds to CHS branches, and the effect of non-uniform connection flexibility on the strength of welds in CHS-to-CHS connections was studied. A total of 24 large-scale, weld-critical experiments was tested and a further 290 non-linear finite element models were used to parametrically expand the database. It was found that if the directional-strength factor is used the target reliability (or safety) index prescribed by AISC for connectors, even when the welds are fully effective, is not achieved; hence, a recommendation to prohibit this factor for all fillet welds around the perimeter of CHS is made. With this restriction, it is then shown that AISC 360-16 Clause J2.4a fillet weld design provisions meet AISC's target safety index for welds in CHS-to-CHS X-connections, where a weld effective length phenomenon exists. It is therefore recommended that AISC advocate 100% weld effective lengths for fillet welds in CHS-to-CHS X-connections, provided that the directional strength-enhancement factor ($1.0+0.5\sin^{1.5}\theta$) is not used.

Key words

Circular hollow section, Fillet weld, Effective length, Connection, Experiment, Finite element

1. Introduction

When welding to hollow structural sections (HSS), welds can be proportioned either: (a) to achieve the capacity of the connected branch member walls, or (b) to be "fit-for-purpose", by considering weld effective lengths (or properties) [1]. By designing welds as "fit-for-purpose" – to resist the actual forces present in the branch member – smaller, more appropriate, and still safe weld sizes can often result.

Over the past 30 years, substantial experimental research efforts have focused on determining weld effective lengths for rectangular hollow section (RHS) connections, including gapped K-connections, T-, Y- and X- (or Cross-) connections, moment-loaded T-connections, and overlapped K-connections [2-6]. Recommendations based on this research have been adopted in North America, by the American Institute of Steel Construction (AISC) in Section K5: "Welds of Plates and Branches to Rectangular HSS" of their latest (2016) steel building specification [7].

When using the weld effective length rules in AISC 360-16 Section K5 to design fillet welds to RHS, the fillet weld directional strength-enhancement factor ($1.0+0.5\sin^{1.5}\theta$) in Clause J2.4b should not be used (i.e. it has been shown, experimentally, that target reliability levels are not achieved) [5, 6, 8-10].

Since the addition of Section K5 (formerly Section K4, in the 2010 specification [11]), weld effective lengths for circular hollow section (CHS) connections have been an issue faced by many code writers, including AISC, since load transfer around a CHS branch can be highly non-uniform [12]. Moreover, the applicability of the ($1.0+0.5\sin^{1.5}\theta$) factor to fillet welds around the perimeter of CHS is unverified. This includes fillet welds in CHS-to-CHS connections, and even fillet welds in CHS-to-rigid plate connections (where the entire weld length is effective), since in both cases bending about the weld axis is unrestrained.

A total of 24 large-scale, weld-critical experiments and 290 non-linear finite element (FE) models was hence investigated to assess the strength of fillet welds around CHS branches, beginning with the applicability of the ($1.0+0.5\sin^{1.5}\theta$) factor to fillet welds in CHS-to-rigid plate connections (Fig. 1a). Weld-critical tests on large-scale, fillet-welded, CHS-to-CHS X-connections (Fig. 1b) were then conducted, and corresponding FE models were developed to determine the adequacy of current AISC 360-16 Section J2.4 weld design provisions.

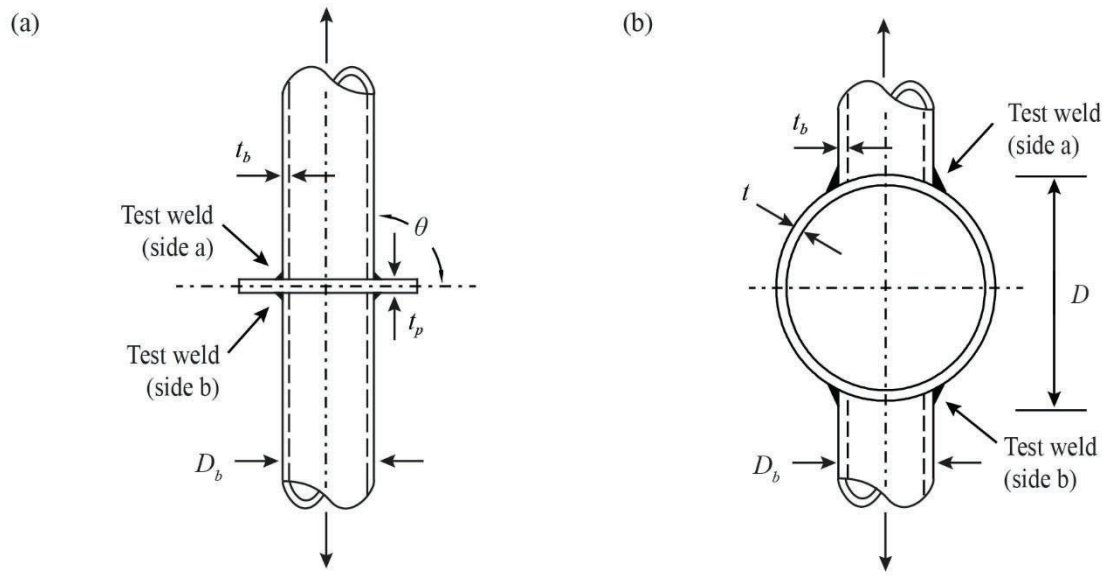

Fig. 1 Experimental test specimens: (a) CHS-to-rigid plate connection; (b) CHS-to-CHS X-connection

2. Fillet welds in CHS-to-rigid plate connections: experiments

2.1. Mechanical and geometrical properties

Six CHS-to-rigid plate connections (Fig. 1a), comprising 12 weld-critical experiments (two per connection), were fabricated from cold-formed CHS made to ASTM A500 Grade C [13] and 25-mm plate with a nominal yield strength of 350 MPa. Fillet welds were made using a semi-automatic flux-cored-arc-welding (FCAW) process with CO_2 shielding gas and an E71T-1C electrode. The average yield stress (F_y) and ultimate stress (F_u, or F_{EXX} for the weld metal) of the CHS, plate and weld metal, determined by tensile coupon testing in accordance with ASTM A370 [14] or AWS D1.1 [15] (for the weld metal) are summarized in Table 1.

Table 1. Measured material properties for the 12 CHS-to-rigid plate experiments

	CHS branch		Plate		Weld metal	
Test No.	F_y MPa	F_u MPa	F_y MPa	F_u MPa	F_y MPa	F_{EXX} MPa
P1, P2, P7, and P8	421	501	409	566	501	571
P3, P4, P9, and P10	431	488	409	566	501	571
P5, P6, P11, and P12	385	450	409	566	501	571

Trial welds were made (prior to fabrication) on identical joints to the CHS-to-rigid plate connections and thereafter sectioned to (a) ensure adequate fusion and (b) set the welding process specification (WPS) for the test connections. A WPS was chosen, from those tested, to produce minimal but just-adequate weld root penetration to allow for accurate characterization of the weld throat dimension(s) (t_w).

Prior to testing, fillet weld faces were ground flat, and leg dimensions on the branch and plate (l_v and l_h) were measured at uniform increments ≤ 30 mm around the CHS perimeter using standard (90° or skew-T) fillet weld gauges. For each pair of leg measurements, t_w was calculated using Eq. (1). Eq. (1) takes into account the effect of unequal leg sizes and the local dihedral angle, ψ (i.e. the angle between the base metal fusion faces), on the orientation of the weld throat plane. For the $\theta = 90°$ connections, $\Psi = 90°$ around the entire joint. For the $\theta = 60°$ connections, Ψ varies continuously around the joint, and it was determined using a method by Luyties & Post [16], programmed in Matlab with measured dimensions of the CHS. In both cases, weld root penetration was ignored because it was shown to be minimal for the chosen WPS.

$$t_w = \frac{l_v l_h \sin\psi}{\sqrt{l_v^2 + l_h^2 - 2 l_v l_h \cos\psi}} \tag{1}$$

The total weld length (l_w), which is used to calculate the weld throat area ($A_w = t_w l_w$), was taken as the CHS contact perimeter, and hence measured along the root of the weld considering the angle between the CHS and the plate. The CHS-to-plate test connection parameters are summarized in Table 2.

Table 2. Measured geometric properties and ultimate loads (experimental and FE) for $\theta = 90°$ and $\theta = 60°$ CHS-to-rigid plate experiments

Test no.		CHS dimensions			Average weld dimensions					
	θ °	$D_b \times t_b$ mm × mm	t_p mm	l_w mm	t_w mm	l_v mm	l_h mm	P_a' kN	P_{FE} kN	P_a'/P_{FE}
P1	90	167.9 × 6.70	25.0	528	4.81	7.04	6.60	1261	1210	1.04
P2					6.63	9.64	9.13	1279	1523	0.84
P3	90	127.4 × 11.55	25.0	401	6.87	9.89	9.54	1459	1337	1.09
P4					7.98	11.23	11.34	1597	1530	1.04
P5	90	101.0 × 7.34	25.0	318	6.38	8.85	9.22	841	860	0.98
P6					6.16	9.23	8.28	864	877	0.99
P7	60	167.9 × 6.70	25.0	569	5.32	6.13	7.41	1450	1207	1.20
P8					5.73	6.88	7.71	1331	1324	1.01
P9	60	127.4 × 11.55	25.0	432	5.21	8.06	8.54	1109	1278	0.87
P10					6.78	10.50	11.13	1479	1601	0.92
P11	60	101.0 × 7.34	25.0	342	5.39	6.93	7.75	776	763	1.02
P12					4.98	6.71	7.32	803	743	1.08

Note: P_a' = greatest actual (experimental) load sustained by the weld; P_{FE} = failure load in the finite element model.

2.2. Test set-up, instrumentation, and results

Quasi-static tension was applied to the ends of the CHS branches by an MTS universal testing machine (UTM), and weld displacement, over a 50-mm gage length, and branch axial strains were measured (Fig. 2a). The branch axial strains were measured at two locations along the branch length: (1) adjacent to the weld, 20 mm from the vertical toe; and (2) in the constant stress region identified by Mehrotra & Govil [17] – a distance of $3D_b$ from the weld toe. These measured strain values were uniform throughout the majority of the tests, indicating that:

(1) the entire weld length was effective (there was uniform loading of the weld); and

(2) the specimens were loaded in pure tension (i.e. there were no bending moments caused by misalignments in the test set-up or by test specimen out-of-straightness).

All 12 test joints failed by weld rupture along a plane through the weld (Fig. 2b). After rupture of one test weld in each connection (e.g. side a), the entire specimen was removed from the UTM and fully re-welded (nominally in the flat position) to ensure separation of the same branch did not occur again. The connection was then tested again, until rupture of the second test weld (e.g. side b) occurred. The ultimate (weld rupture) loads (P_a') are given in Table 2.

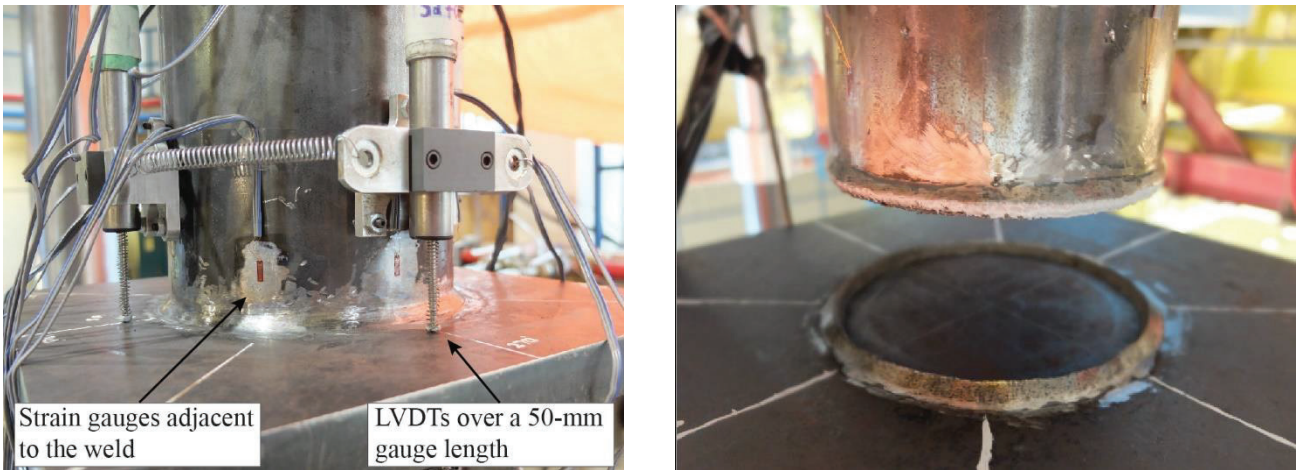

(a) (b)

Fig. 2 CHS-to-rigid plate (a) instrumentation adjacent to the test weld, and (b) typical weld rupture failure mode

3. Fillet welds in CHS-to-rigid plate connections: finite element modelling

The 12 CHS-to-rigid plate experiments were used to validate FE models in ANSYS 14.0 [18]. Unlike the experiments, the models were each comprised of a *single* tension-loaded branch welded to a rigid plate, with nodes restrained on the "underside" of the plate (preliminary FE modelling indicated results were equivalent to modelling the full specimens). Either one quarter or half of the FE connection was modelled using appropriate symmetry boundary conditions depending on the branch angle (θ = 90° or 60°, respectively). A θ = 90° model is shown in Fig. 3. To restrict load transfer to the fillet weld, a 0.25-mm gap was modelled between the CHS and the plate. The size of this gap was selected to minimize its effect on the relationship between l_v, l_h, and t_w. These, and all subsequent FE models, were analyzed under static incremental displacements applied to the branch in the theoretical constant stress region ($3D_b$ from the weld toe).

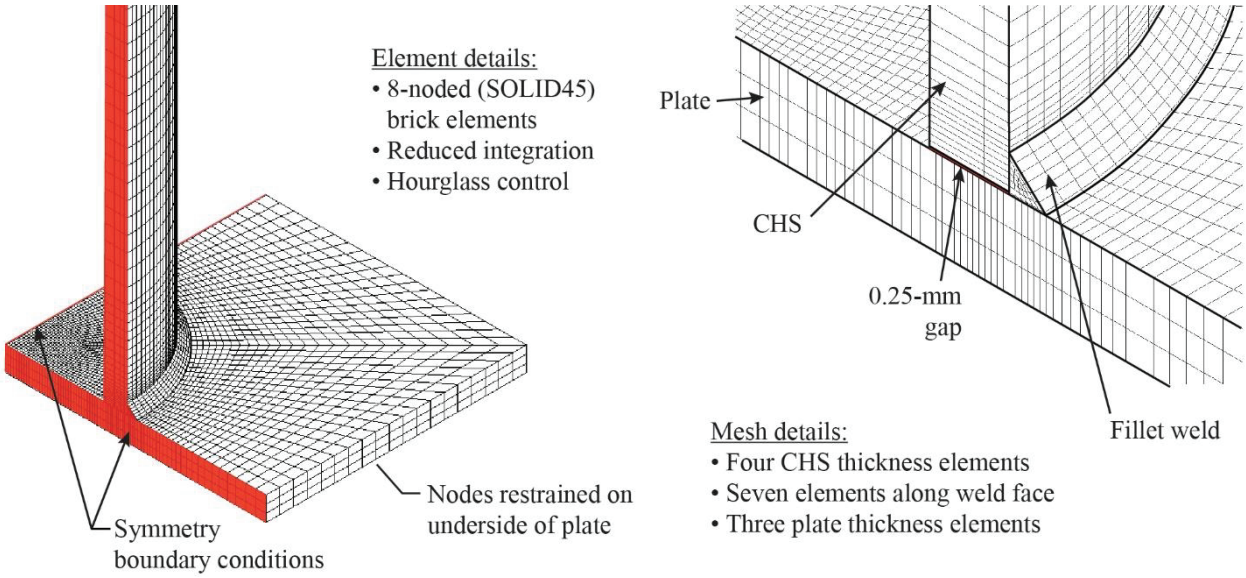

Fig. 3 CHS-to-rigid plate FE model with $\theta = 90°$ and key element and mesh details

3.1. Material modelling

Multi-linear true stress-strain curves for each different material (i.e. the weld metal, plate, and each different branch member) were derived from tensile coupon (TC) tests conducted in accordance with ASTM A370 [14]. Prior to necking, the average engineering stress (σ) and strain (ε) ordinates from the tests were converted to true stress (σ_T) and strain (ε_T) using the following relationships [19]:

$$\sigma_T = \sigma(1+\varepsilon) \tag{2}$$

$$\varepsilon_T = \ln(1+\varepsilon) \tag{3}$$

After necking, an iterative approach based on matching the engineering stress-strain curve of a coupon modelled in ANSYS to that of an experimental test was used to determine ordinates on the σ_T-ε_T curves [20]. The trial-and-error approach involves weighting approximate lower- and upper-bounds to the σ_T-ε_T response. The same elements later employed for the CHS-to-rigid plate models (8-noded brick elements), with large deformations and non-linear material properties, were used. The results of a sensitivity study performed to determine the element type and mesh

arrangement best suited for modelling the full-scale CHS-to-rigid plate connections (i.e. the element and mesh details used) are listed in Fig. 3, shown previously.

3.2. Model fracture criterion

The ANSYS "element death feature" was used to simulate fracture in the fillet welds and/or the plate, which was triggered by a maximum equivalent strain fracture criterion (ε_{ef}) [21, 22].

The maximum equivalent strain fracture criterion (ε_{ef}) was determined by comparing the load-displacement results from six CHS-to-rigid plate FE analyses to corresponding experimental results. By trial and error, the correct value of ε_{ef} for rupture in the weld ($\varepsilon_{ef,weld}$) was determined to be the one that matched the FE and experimental displacement (over the 50-mm gauge length) at weld fracture. Using displacement instead of load to calibrate $\varepsilon_{ef,weld}$ provided more accurate results (in terms of actual-to-predicted fracture loads *and* displacements) because weld rupture typically occurred on the plateau of the load-displacement curve.

The mean value of $\varepsilon_{ef,weld}$ obtained for the six tests was 0.092. This value was used as the criterion to initiate the ANSYS element death feature to reduce the stiffness of an element to nearly zero. The inactive element(s) thereafter sheds load to the surrounding elements (where the equivalent strain, $\varepsilon_e < \varepsilon_{ef}$) and freely deforms. This behaviour is physically comparable to the initiation and propagation of a crack through the weld. An equivalent strain fracture criterion for elements in the plate ($\varepsilon_{ef,plate} = 0.011$) was also calibrated, and determined from five previous tests on RHS-to-rigid plate connections by Frater [23] that failed in this manner (by plate rupture).

3.3. Model validation

The ultimate load predicted by the FE models (P_{FE}) for all 12 CHS-to-rigid plate experiments is shown in Table 2 (presented previously). It can be seen that the models provided good predictions of P_a'. The mean of the ratio of actual-to-predicted ultimate loads in Table 2 (P_a'/P_{FE}) is 1.01, with a coefficient of variation (COV) of 0.10.

The FE load-displacement curves are compared to the experimental curves in Fig. 4 for six (out of the 12) tests. Even though weld penetration was ignored (because it was shown to be minimal for the chosen WPS) and average

values of the weld dimensions (t_w, l_v and l_h) were used, the FE and experimental load-displacement curves show good agreement.

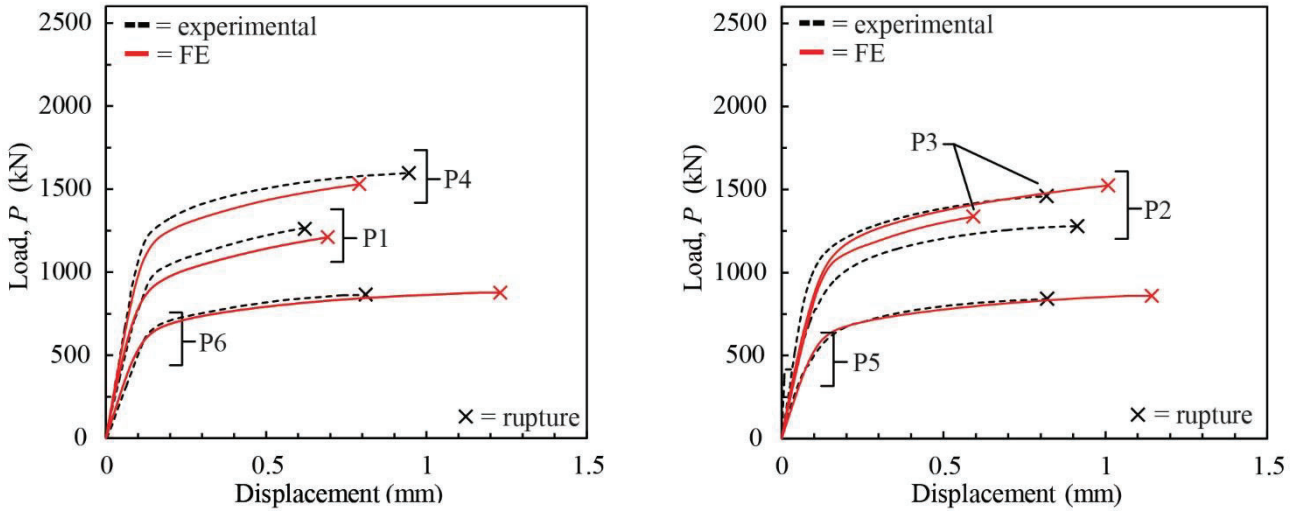

Fig. 4 Comparison of CHS-to-rigid plate FE and experimental load-displacement responses: (a) test nos. P1, P4 and P6; (b) test nos. P2, P3 and P5

3.4. Parametric study

An FE parametric study was thus conducted to extend the database in which the ratio of weld size to branch thickness (t_w/t_b = 0.35, 0.50, 0.71, 0.90, and 1.06) and the CHS branch slenderness (D_b/t_b = 9.1, 12.5, 20, 30, 40, and 50) were varied. For these FE models, θ = 90°; however, four additional FE models (with t_w/t_b = 0.50, D_b/t_b = 12.5 or 50, and θ = 60° or 75°) were later analysed to determine the effect of branch inclination angle on the weld strength. In all models, fillet welds were modelled with equal-sized legs, and the same CHS diameter and plate thickness were used (D_b = 168 mm and t_p = 25 mm). Additionally, the same set of material properties were used (for the weld, the CHS, and the plate). These were taken as the most nominally matched weld and base metal materials from the CHS-to-rigid plate experiments (i.e. test nos. P1, P2, P7, and P8 in Table 1).

3.4.1. Results of the parametric study

Weld rupture occurred in 25 (out of the 30) parametric CHS-to-rigid plate models with $\theta = 90°$. In five of these 25 tests, the branch yielded before the weld ruptured; hence, 20 of these tests were weld-critical. Failure modes, and the non-dimensional average stress on the weld throat at failure (P_{FE}/A_wF_{EXX}, herein called the weld strength), are summarized in Table 3. Table 3 shows that in general the weld strength decreases as both t_w/t_b and D_b/t_b increase.

Table 3. Non-dimensional parameters, P_{FE}/A_wF_{EXX}, and failure mode for CHS-to-rigid plate FE analyses

		t_w/t_b				
t_b	D_b/t_b					
mm		0.35	0.50	0.71	0.90	1.06
3.36	50	0.85 W	0.87 W	0.81 W	0.76 W	0.73 W †
4.20	40	0.89 W	0.86 W	0.82 W	0.76 W	0.73 W †
5.59	30	0.88 W	0.88 W	0.82 W	0.78 W	0.74 W †
8.40	20	0.90 W	0.88 W	0.85 W	0.80 W †	0.76 W †
13.44	12.5	0.93 W	0.89 W	0.87 W	0.79 P †	0.71 P †
18.48	9.1	0.92 W	0.90 W	0.83 P	0.71 P†	0.65 P †

Note: W = rupture through the weld; P = rupture only in the plate.
† Branch yielded before weld ruptured.

Based on a comparison of the results of the four additional FE models (with $\theta = 60°$ or 75°) to $\theta = 90°$ models with the same values of t_w/t_b and D_b/t_b (Fig. 5), it is shown that while the $(1.0+0.5\sin^{1.5}\theta)$ factor predicts a reduction in weld strength as the average loading angle of the weld θ goes from 90° to 60°, this is not the case for CHS-to-rigid plate connections. The forthcoming reliability analysis is therefore concerned with applicability of the $(1.0+0.5\sin^{1.5}\theta)$ factor only to CHS-to-rigid plate connections with $\theta = 90°$, since the above evidence suggests it does not predict the correct trend when θ is less than 90°.

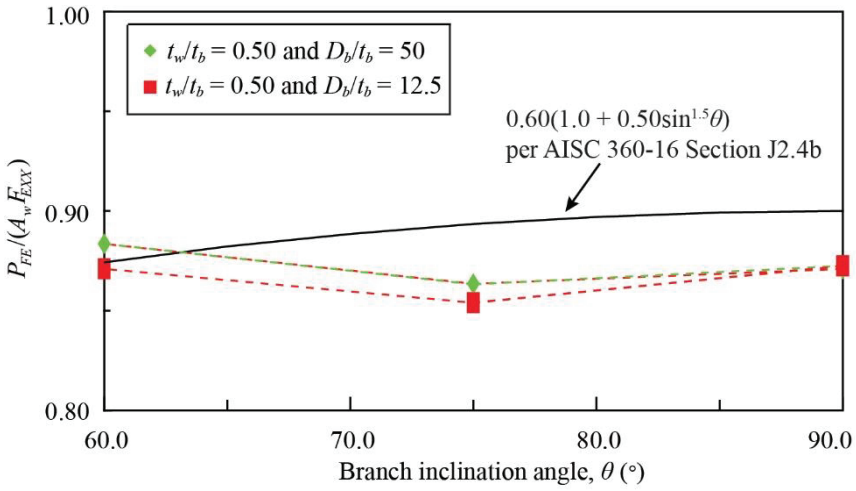

Fig. 5 Effect of branch inclination angle on fillet weld strength in CHS-to-rigid plate connections

4. Evaluation of the (1.0+0.5sin$^{1.5}\theta$) factor for fillet welds to CHS branches

4.1. Existing AISC 360-16 provisions for design of fillet welds to CHS branches

According to AISC 360-16 Section J2.4a, the nominal strength of a fillet weld (P_n) is based on the limit state of shear rupture along the plane of the weld effective throat in accordance with Eq. (4):

$$P_n = 0.60 F_{EXX} A_w \tag{4}$$

where A_w = the effective weld throat area (= $t_w l_w$).

An LRFD resistance factor for fillet welds, ϕ, equal to 0.75, is then applied to determine the design (available) strength.

For parallel weld elements with a uniform leg size, loaded through the centre of gravity, AISC 360-16 Section J2.4b permits the use of the (1.0+0.5sin$^{1.5}\theta$) factor when determining P_n. Thus:

$$P_n = 0.60(1.0 + 0.50\sin^{1.5}\theta) F_{EXX} A_w \tag{5}$$

where θ = angle of loading measured from the weld longitudinal axis (in degrees).

Either Eq. (4) or (5) could be used to design fillet welds around the perimeter of a CHS welded to a rigid plate.

4.2. Safety level inherent in AISC 360-16 fillet weld design provisions

To assess whether adequate safety margins are inherent in the $(1.0+0.5\sin^{1.5}\theta)$ factor for fillet welds in CHS-to-rigid plate connections, the structural reliability (or safety index) (β^+) can be calculated, and compared to the target value of 4.0 (per Section B3.1 of the AISC 360-16 Commentary), using a simplified reliability analysis in which the resistance factor, ϕ, is given by Eq. (6) [24, 25]:

$$\phi = \phi_{\beta+}\rho_R e^{-\alpha_R \beta^+ V_R} \tag{6}$$

where α_R = coefficient of separation taken as 0.55 [24]; ρ_R = bias coefficient for resistance (mean ratio of actual-to-predicted weld strength); V_R = associated coefficient of variation (COV) of ρ_R; and $\phi_{\beta+}$ = adjustment factor for β^+ that is needed when $\beta^+ \neq 3.0$ [25]. A formula for $\phi_{\beta+}$ was derived by Franchuk et al. [26]:

$$\phi_{\beta+} = 0.0062(\beta^+)^2 - 0.131\beta^+ + 1.338 \tag{7}$$

The mean actual-to-predicted weld strength ratio (ρ_R) was taken as the average over all of the $\theta = 90°$ weld-critical tests of P_a' (or P_{FE}) divided by P_n, with P_n calculated using Eq. (5), and the measured values of A_w and F_{EXX}. The reliability analysis parameters, and the results of the reliability analysis, are shown in Table 4. The implied safety index, β^+, = 3.69 < 4.0 for Eq. (5). This indicates that the AISC 360-16 Section J2.4b formula is unsafe for fillet welds to CHS branches when the welds are fully effective. Fig. 6a shows the correlation of the existing AISC 360-16 predicted nominal strengths using Eq. (5) with the FE and experimental results.

Table 4. AISC 360-16 reliability analysis parameters (CHS-to-rigid plate experiments and FE analyses)

	Section J2.4b $P_n = 0.60(1.0+0.50\sin^{1.5}\theta)F_{EXX}A_w$	Section J2.4a $P_n = 0.60F_{EXX}A_w$
number of tests	26	26
ϕ	0.75	0.75
ρ_R	0.94	1.41
V_R	0.08	0.08
ϕ_{β^+}	0.94	0.72
β^+	3.69 < 4.0	7.01 ≥ 4.0

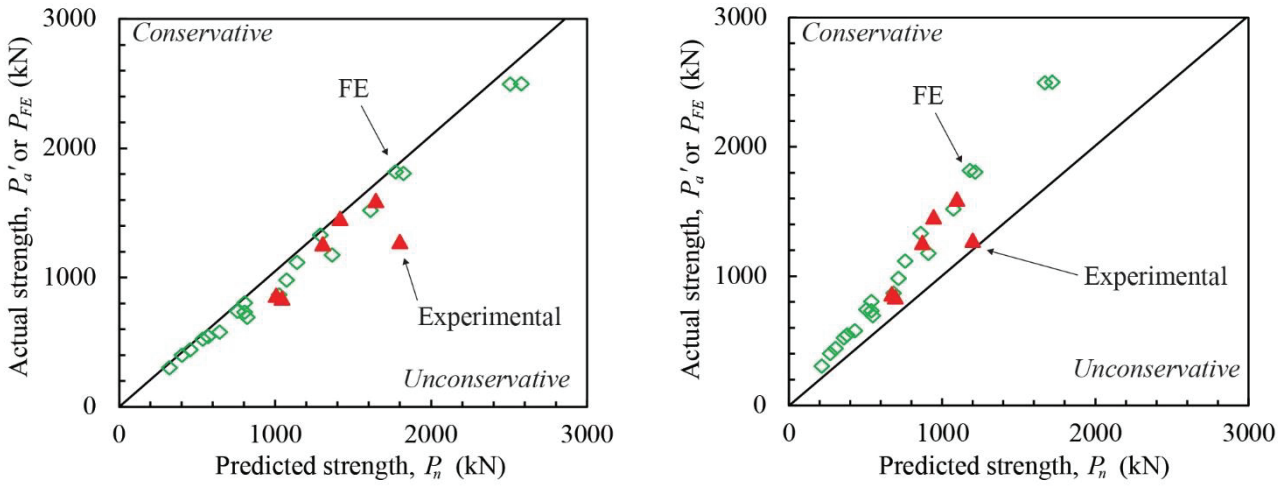

Fig. 6 Correlation of AISC 360-16 fillet weld design provisions with 26 weld-critical $\theta = 90°$ CHS-to-rigid plate test results: (a) Section J2.4b [with the $(1.0+0.5\sin^{1.5}\theta)$ factor]; (b) Section J2.4a [without the $(1.0+0.5\sin^{1.5}\theta)$ factor]

If the reliability analysis is repeated with P_n calculated using Eq. (4) [i.e. omitting the $(1.0+0.5\sin^{1.5}\theta)$ factor], the correlation in Fig. 6b results, and the implied safety index, $\beta^+ = 7.01 > 4.0$ (Table 4). It can therefore be concluded that, for fillet-welded CHS-to-rigid plate connections in which the welds are fully effective, the provisions of AISC 360-16 Section J2.4b should not be used. It follows that the $(1.0+0.5\sin^{1.5}\theta)$ factor should also not be used with CHS branches when fillet welds are partially effective, such as in CHS-to-CHS connections.

5. Fillet welds in CHS-to-CHS X-connections: experiments

5.1. Mechanical and geometrical properties

Six CHS-to-CHS X-connections, comprising 12 weld-critical experiments (two per connection), were designed and fabricated from ASTM A500 [13] dual-certified Grade B/C cold-formed CHS, and fillet welded using the same FCAW process used for the CHS-to-rigid plate connections. The CHS members were selected to cover a wide range of branch-to-chord diameter ratios ($\beta = D_b/D$), chord wall slenderness values (D/t), and branch inclination angles (θ) (Table 5), within Ψ limits for fillet welds to develop the full throat thickness without Z-loss ($60° < \Psi < 120°$, according to AWS D1.1-15). Branches were a minimum length (l_b) of $6D_b$ to avoid shear lag effects at the connection [17], and profiled to saddle perfectly onto the chords, without edge bevelling. The chords were a minimum length (l) to avoid end effects at the connection [27], and left uncapped.

Table 5. Measured geometric properties and ultimate loads (experimental and FE) for $\theta = 90°$ and $\theta = 60°$ CHS-to-CHS X-connection experiments

Test no.	CHS branch	CHS chord		Average weld dimensions							
	$D_b \times t_b$	$D \times t$	θ	l_w	t_w	l_v	l_h	P_a	P_a'	P_{FE}	P_a'/P_{FE}
	mm × mm	mm × mm	°	mm	mm	mm	mm	kN	kN	kN	
X1	102.0 × 7.34	273.5 × 11.69	90	322	4.08	6.86	6.17	672	672	655	1.03
X2	102.0 × 7.34	273.5 × 11.69		322	4.37	7.23	6.65	678	678	690	0.98
X3	102.0 × 7.34	406.5 × 12.34		320	3.56	5.16	5.78	608	608	543	1.12
X4	102.0 × 7.34	406.5 × 12.34		320	3.14	4.54	5.08	540	540	495	1.09
X5	127.4 × 11.55	273.5 × 11.69		406	3.63	5.94	5.93	653	653	762	0.86
X6	127.4 × 11.55	273.5 × 11.69		406	4.00	7.05	6.06	609	653	811	0.80
X7	127.4 × 11.55	406.5 × 12.34		403	3.16	4.83	5.03	557	557	631	0.88
X8	127.4 × 11.55	406.5 × 12.34		403	3.47	5.60	5.19	556	557	617	0.90
X9	102.0 × 7.34	410.0 × 12.21	60	345	3.58	5.83	5.59	721	721	640	1.13
X10	102.0 × 7.34	410.0 × 12.21		345	3.79	6.29	5.83	538	721	672	1.07
X11	127.4 × 11.55	410.0 × 12.21		434	3.95	5.68	8.01	761	761	903	0.84
X12	127.4 × 11.55	410.0 × 12.21		434	3.38	5.39	6.00	798	850	798	1.06

Note: P_a = actual (experimental) load at weld rupture; P_a' = greatest actual (experimental) load sustained by the weld; P_{FE} = failure load in the finite element model.

Welds were again ground flat, and components of l_v and l_h parallel to the branch axis were measured at 12 or 15 different locations along the weld length (for branches with D_b = 102.0 or 127.4 mm, respectively). These measurements were used to model the 3D weld around the entire joint in Solidworks, with actual measured values of D_b and D. Sections were then cut through the weld (in Solidworks), in the plane of Ψ (i.e. the plane normal to the weld throat dimensions) so that the correct values of l_v, l_h and t_w could be measured (Fig. 7). The total weld length (l_w), and the weld length tributary to each cut through the weld, were calculated by modifying Luyties & Post's [16]

method for calculating Ψ to give a near-perfect solution for the distance between points along the weld length (and then summing up these distances). The weld area (A_w) was hence taken as the sum of: (t_w × tributary weld length) around the entire joint.

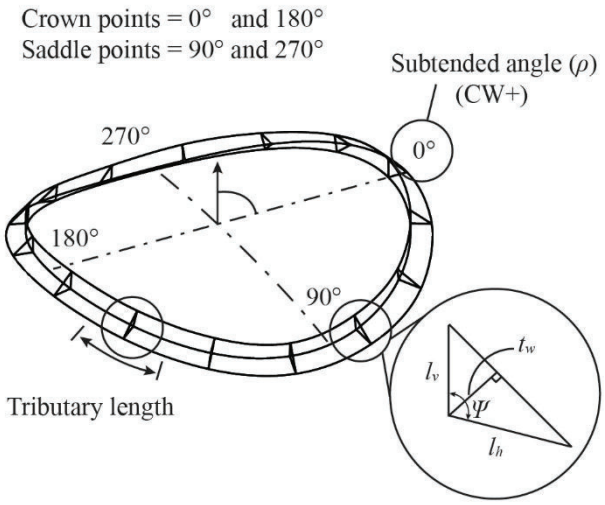

Fig. 7 3D weld and section cuts (in Solidworks)

The average yield stress (F_y) and ultimate stress (F_u, or F_{EXX} for the weld metal) of the CHS branches, chord, and weld metal, determined by tensile coupon testing in accordance with ASTM A370 [14] or AWS D1.1 [15] (for the weld metal), are summarized in Table 6.

Table 6. Measured material properties for the 12 CHS-to-CHS X-connection experiments

	CHS branch		CHS chord		Weld metal	
Test No.	F_y MPa	F_u MPa	F_y MPa	F_u MPa	F_y MPa	F_{EXX} MPa
X1 and X2	373	454	460	540	517	577
X3 and X4	373	454	355	464	517	577
X5 and X6	431	488	460	540	517	577
X7 and X8	431	488	355	464	517	577
X9 and X10	373	454	373	485	517	577
X11 and X12	431	488	373	485	517	577

5.2. Test set-up and instrumentation

Quasi-static axial tension was applied to the end of each branch on either side of the connection, and hence to the weld, by the same MTS UTM used previously for the CHS-to-plate tests. The testing arrangement, shown in Fig. 8a, consisted of the following instrumentation:

(a) four linear strain gauges (SGs) equally spaced around the perimeter of one branch, at mid length, which confirmed uniform tensile loading of the branch;

(b) seven additional SGs with the same orientation, 20 mm away from the weld toe around half the weld perimeter (i.e. on one side of the branch only, due to symmetry) that monitored non-uniform loading of the weld (Fig. 8b); and

(c) an LED scanner, with three LED targets (one on each branch, 50 mm above the crown, and one at the connection work point on the chord face parallel to the plane of the connection) that monitored chord deformation (δ) throughout each test (see Fig. 8a).

The value of δ, which is the outward displacement (normal to the chord) of a single branch from the chord centreline [28], was taken as half of the vertical displacement between the LEDs on each branch. It therefore represents the average deformation on both sides of the connection.

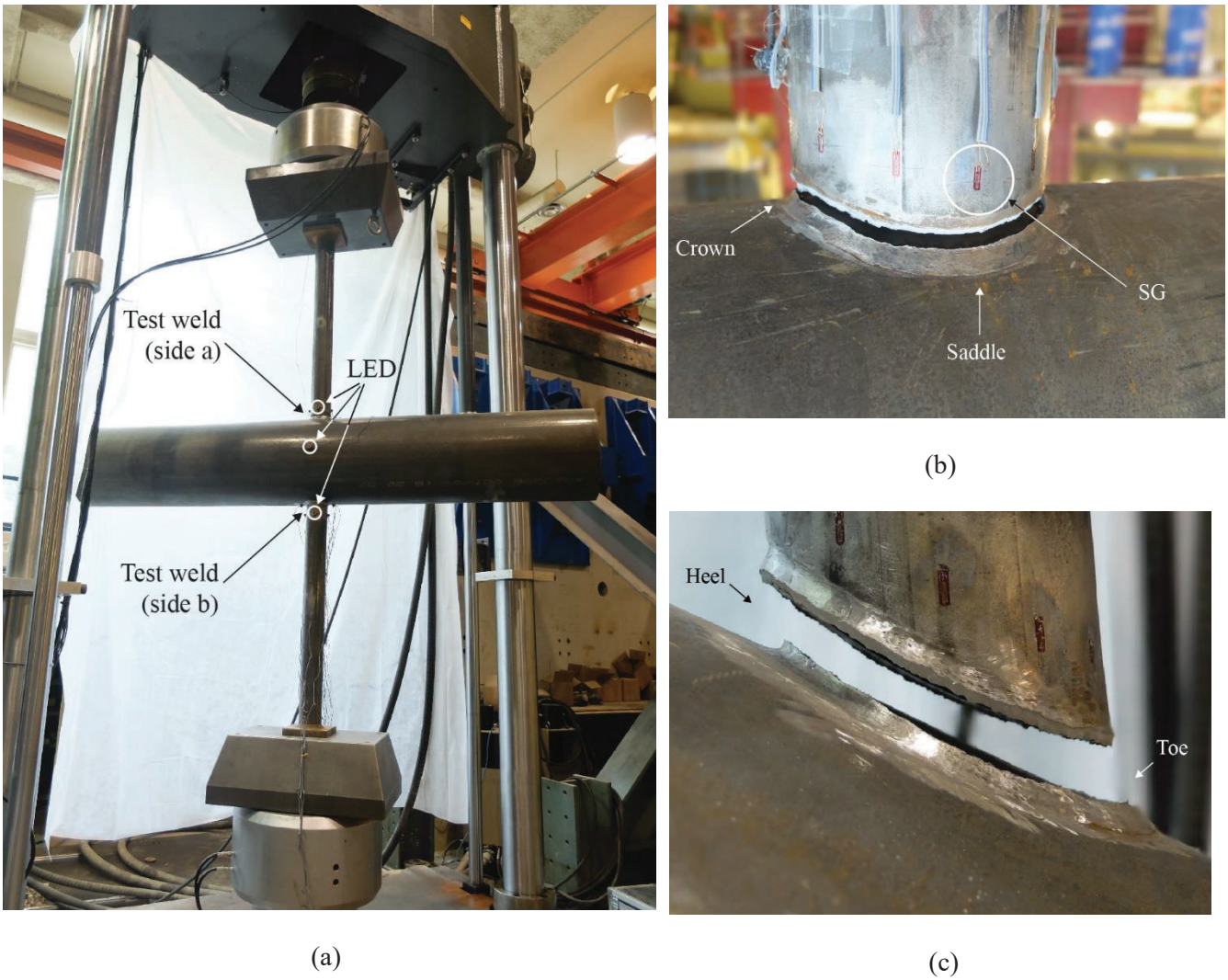

(a) (b) (c)

Fig. 8 CHS-to-CHS X-connection experiments: (a) testing arrangement; (b) weld fracture in test no. X5 (θ = 90°); and (c) weld fracture in test no. X9 (θ = 60°)

The procedure used for the CHS-to-plate tests to rupture both welds in the connection was again used for the CHS-to-CHS tests. All 12 test joints failed by weld rupture along a plane through the weld (Fig. 8b,c). The weld ultimate loads (P_a' in Table 5) were measured using a load cell in-line with the UTM actuator, and taken as the greatest load sustained by the weld (even if weld rupture occurred at a lower load during a later loading). The column P_a in Table 5 gives the actual load at weld rupture.

5.3. Results

Representative graphs of the strain distribution around the branch adjacent to the test weld, for various levels of applied load, are given in Fig. 9. For $\theta = 90°$ connections (Fig. 9a), the tensile strain (and hence tensile load) peaks at the saddle point ($\rho = 90°$). Demand on the weld is smallest at the crown points ($\rho = 0°$ and 180°); much of the weld even remained in compression for the majority of the tests. This phenomenon equates to a non-uniform loading of the weld perimeter, and indicates that weld effective lengths are present in CHS-to-CHS connections.

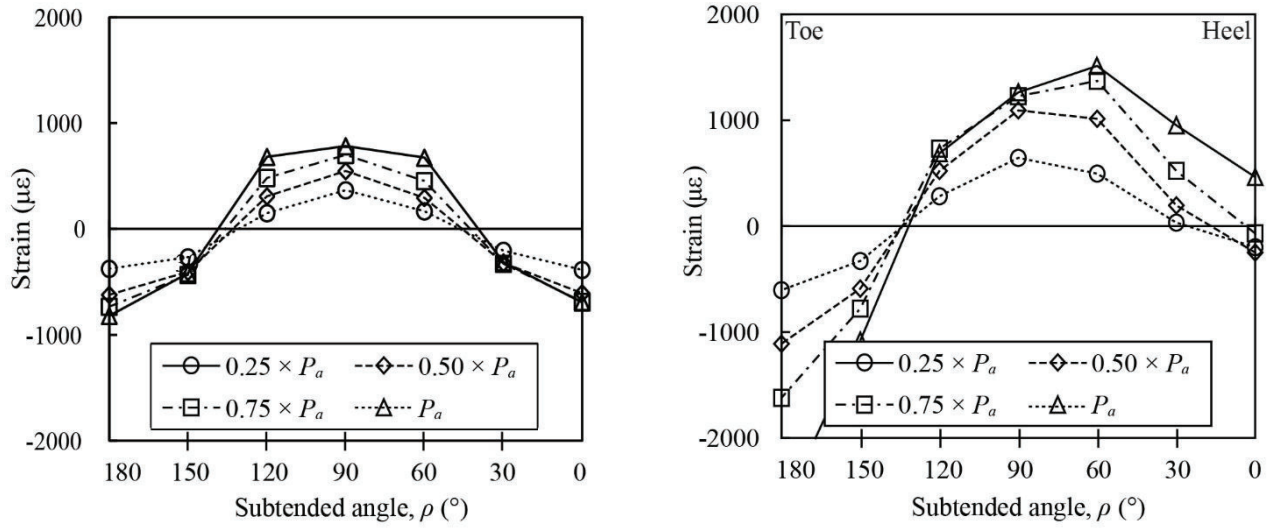

(a) (b)

Fig. 9 Typical strain distributions adjacent to test welds: (a) test no. X7 ($\theta = 90°$), (b) test no. X9 ($\theta = 60°$)

For $\theta = 60°$ connections, the peak tensile strain is initially at the saddle point ($\rho = 90°$) (Fig. 9b), but moves towards the heel as the load increases. This may be due to secondary bending effects from connection flexibility and joint rotation which do not exist in real structures when the chord ends are prevented from moving because they are connected to other members.

6. Fillet welds in CHS-to-CHS X-connections: finite element modelling

CHS-to-CHS X-connection FE models were hence developed to replicate the experimental tests and extend the test database. The models were developed using the same approach as the CHS-to-rigid plate connections, including

use of a 0.25-mm gap between the branches and the chord. Although it was possible to model just one eighth of the non-inclined ($\theta = 90°$) connections due to symmetry about three principal planes passing through the work point, one half of every connection was modelled instead to accommodate the inclined branch ($\theta < 90°$) cases. The element and mesh details used were the same as those for the CHS-to-plate FE tests; these are depicted in Fig. 10, and were shown to be suitable by conducting a separate sensitivity study.

An FE fracture criterion for the weld ($\varepsilon_{ef,weld} = 0.32$) was applied to only one weld in the connection (i.e. the "critical weld" in Fig. 10). The difference in $\varepsilon_{ef,weld}$ between the CHS-to-CHS X-connections ($\varepsilon_{ef,weld} = 0.32$) and the CHS-to-rigid plate connections ($\varepsilon_{ef,weld} = 0.092$) is due to different triaxiality at the location of rupture [21, 29], and is expected. Base metal rupture was not observed in any tests, and was hence not included in the model.

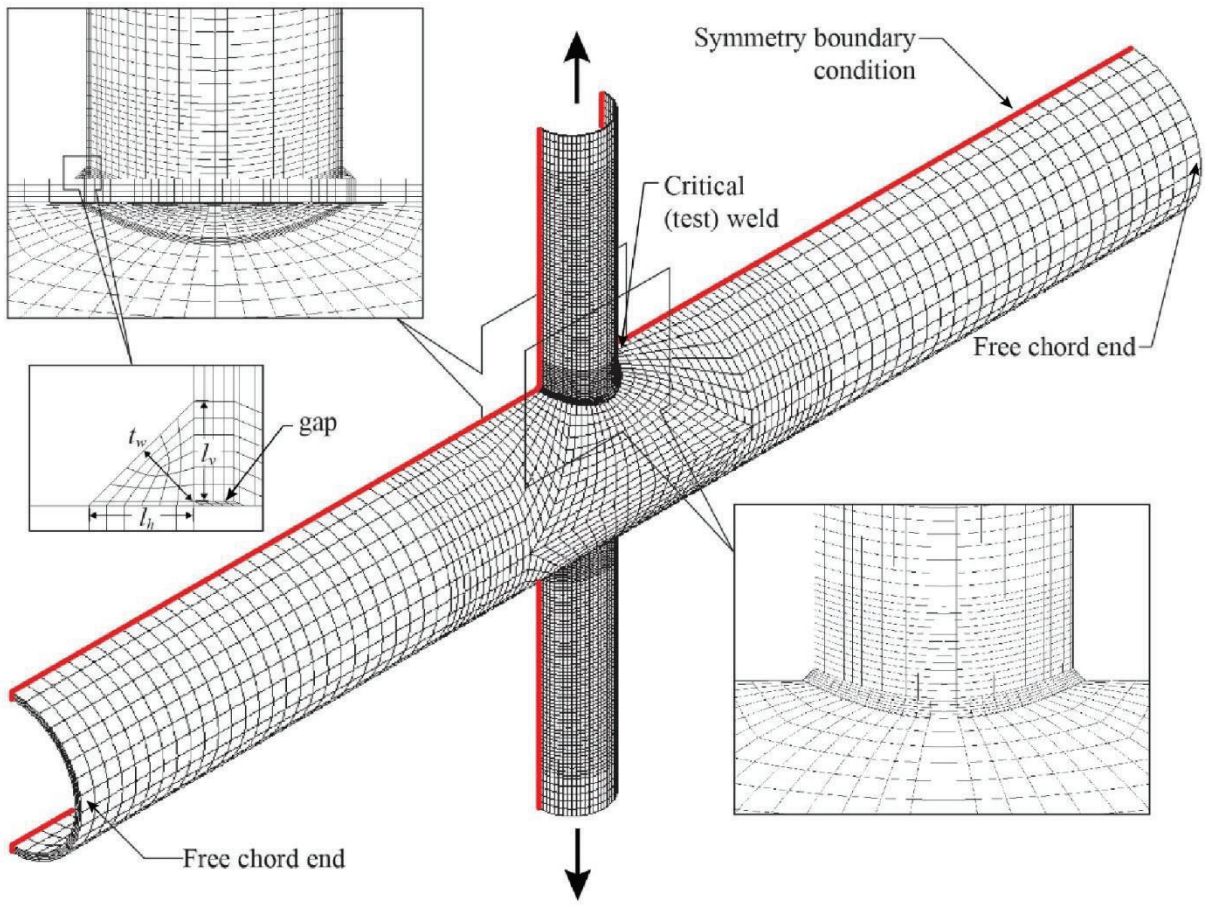

Fig. 10 CHS-to-CHS FE model with $\theta = 90°$

6.1. Model validation

Fig. 11a,b compares the experimental and FE load-deformation curves for six (of the 12) specimens. The deformations have been normalized, by dividing by D, so that curves for connections with different chord diameters can be compared on the same plot. For clarity, the six curves have been divided between two graphs. Despite the same assumptions made for the CHS-to-plate FE models (weld penetration was ignored and average values of the weld dimensions were used), the FE and experimental load-displacement curves show good agreement. In Table 5 (shown previously) the mean actual-to-FE predicted ultimate load (P_a'/P_{FE}) is 0.98, with a coefficient of variation (COV) of 0.12. These values indicate that the model made acceptable predictions of P_a' across all tests.

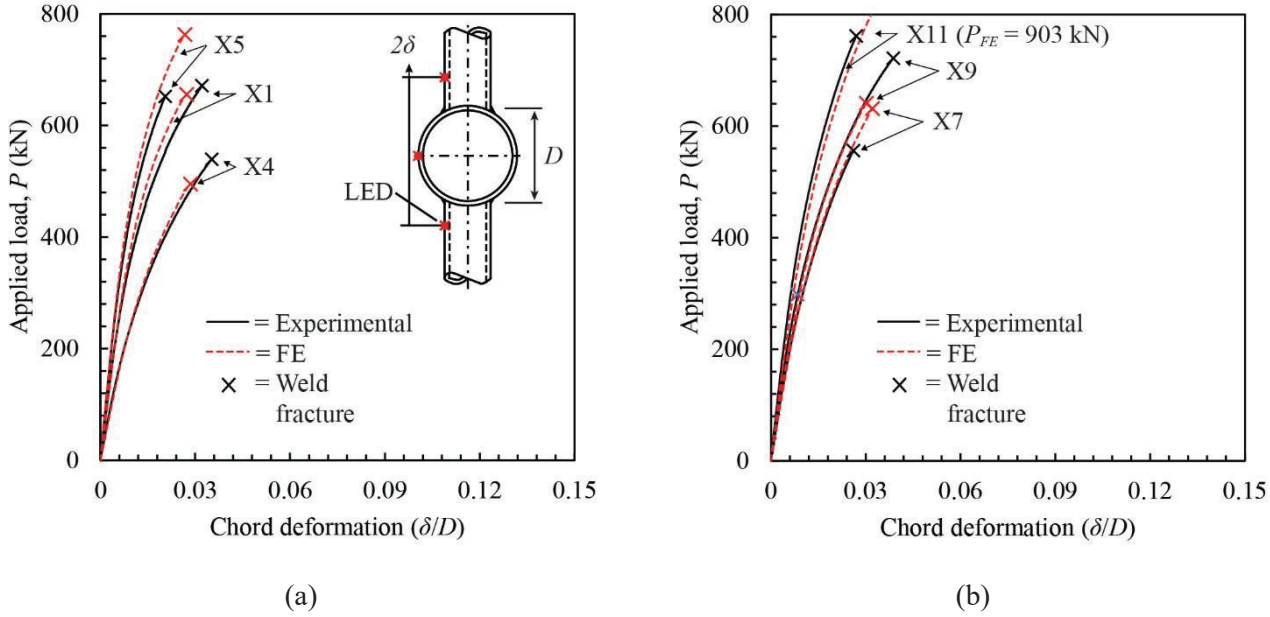

Fig. 11 Comparison of CHS-to-CHS FE and experimental load-displacement responses: (a) test nos. X1, X4 and X5; (b) test nos. X7, X9 and X11

6.2. Parametric study

A range of non-dimensional connection parameters was chosen to cover all permissible fillet-welded connections subject to the following restrictions: (a) the local dihedral angle (Ψ) limits imposed by AWS D1.1-15 Fig. 9.10 and Table 9.5 ($60° \leq \Psi \leq 120°$); (b) the limits of applicability of connection design formulae in AISC 360-16 Table K3.1, which are given in AISC 360-16 Table K3.1A; and (c) the range of standard CHS sections available

for designers in Table 1-13 of the *Steel Construction Manual* [30]. The parameters varied were: the branch inclination angle (θ = 60°, 70°, 80°, and 90°); the chord slenderness (D/t = 10, 20, 30, 40, and 50); the branch-to-chord diameter ratio (β = 0.10, 0.20, 0.30, 0.40, and 0.50); and the branch-to-chord thickness ratio (τ = 0.20, 0.40, 0.60, 0.80, and 1.00). Although a total of 500 permutations exist for the values given, there are several practical limitations that must be considered. First, available CHS sections limit branch slenderness ratios (D_b/t_b) to between about 10 and 50. Secondly, not all combinations of β and θ produce Ψ between 60° and 120° (to qualify as a fillet weld) along the entire weld length. A comprehensive parametric study was hence performed by modelling β up to 0.30 for 60° connections and β up to 0.50 for all other branch angles. A total of 256 CHS-to-CHS X-connection models was thus analysed.

6.2.1. Details of the parametric models

The CHS-to-CHS X-connection parametric FE models had constant branch diameters (D_b) of 200 mm and $t_w = 0.50t_b$ to ensure that the branch yield capacity was not reached before weld fracture. As in the experiments, the ends of the chords were uncapped. The length of the chord (l) was $10D$ (when $D/t > 25$) or $6D$ (when $D/t \leq 25$) to prevent chord end effects at the connection (i.e. the effect of the chord end conditions – fixed, pinned, or free, capped or uncapped – on the connection load-displacement response) [27]. The length of the branches (l_b) was $3D_b$, and load was applied to their ends in the theoretical constant stress region [17]. All models used the same set of material properties (for the weld, the branches, and the chord) taken as the most nominally matched weld and base metals from the CHS-to-CHS experiments in Table 6 (i.e. test nos. X5 and X6).

6.2.2. Results of the parametric study

All 256 FE analyses failed by weld fracture while the branches of the connection remained elastic. Fracture initiated in the weld at the saddle point and propagated away from the saddle towards the crown before the maximum load was reached. It was found from these 256 analyses that the weld strength (P_{FE}/A_wF_{EXX}) decreases as D/t, β and τ increase. The branch inclination angle was found to have no significant effect.

7. Evaluation of AISC 360-16 fillet weld design provisions for CHS-to-CHS X-connections

The previous reliability analysis was repeated using all 268 experimental and FE CHS-to-CHS X-connection results to determine the implied safety index, β^+, for the current AISC 360-16 provisions *without* weld effective lengths (i.e. using Section J2.4a). The mean actual-to-predicted weld strength ratio (ρ_R) was hence taken as the average over all tests of P_a' (or P_{FE}) divided by P_n, with P_n calculated using Eq. (4), and the measured values of A_w and F_{EXX}. The analysis determined that $\beta^+ = 4.53 \geq 4.0$ for AISC 360-16 without weld effective lengths. Table 7 summarizes the reliability analysis parameters. A correlation plot is presented in Fig. 12.

Table 7. AISC 360-16 reliability analysis parameters (CHS-to-CHS experiments and FE analyses)

	Section J2.4a $P_n = 0.60F_{EXX}A_w$
number of tests	268
ϕ	0.75
ρ_R	1.38
V_R	0.19
ϕ_{β^+}	0.87
β^+	$4.53 \geq 4.0$

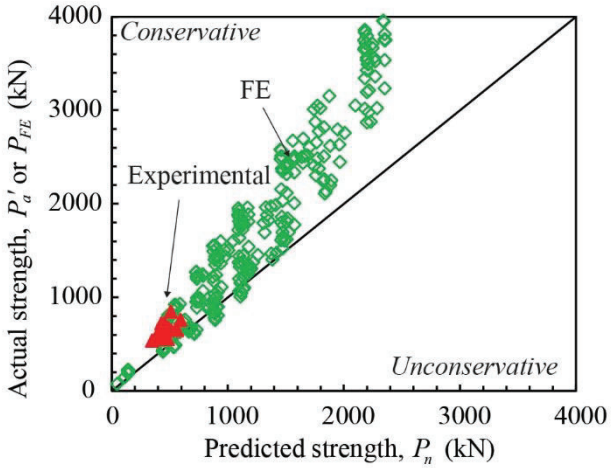

Fig. 12 Correlation of AISC 360-16 Section J2.4a fillet weld design provisions with 268 weld-critical CHS-to-CHS test results

It can therefore be concluded that weld effective lengths are not required for fillet-welded CHS-to-CHS X-connections in conjunction with the AISC 360-16 Section J2.4 code design method, provided that the $(1.0+0.50\sin^{1.5}\theta)$ factor (given in Section J2.4b) is not used.

8. Conclusions and recommendations

Based on 12 experiments and 34 FE analyses on fillet-welded CHS-to-rigid plate connections, it was shown that the $(1.0+0.5\sin^{1.5}\theta)$ factor in AISC 360-16 Section J2.4b fails to provide an adequate reliability (safety) index ($\beta^+ = 3.69 < 4.0$) for fillet welds around CHS branches.

Based on 12 further experiments and 256 further FE analyses on fillet-welded CHS-to-CHS X-connections, it was shown that the current AISC 360-16 Section J2.4 specification provisions for fillet welds provide adequate structural reliability ($\beta^+ = 4.53 \geq 4.0$) without weld effective lengths (i.e. when the total weld length is used to determine the weld strength), provided that the $(1.0+0.50\sin^{1.5}\theta)$ factor is not used. This is because the analysis method of AISC 360-16 Section J2.4 considers the axial force in the branch member to be resisted only by shear stress on the weld throat, which is a conservative assumption.

It is therefore recommended that the provisions of AISC 360-16 Section J2.4 be used without the $(1.0+0.50\sin^{1.5}\theta)$ factor [i.e. taking $\theta = 0°$ in the term $(1.0+0.50\sin^{1.5}\theta)$] for *all* fillet welds around the perimeter of CHS branches (including CHS-to-CHS connections, where weld effective lengths are theoretically present, and CHS connections in which the welds are fully effective, e.g. CHS-to-rigid plate connections). Furthermore, it is recommended that AISC advocate 100% weld effective lengths for fillet-welded CHS-to-CHS X-connections, subject to the above restriction on the $(1.0+0.50\sin^{1.5}\theta)$ factor.

Acknowledgements

The authors would like to acknowledge the laboratory contributions of Ms. J. Lu and Mr. F. Wei (summer research students) to this work. Hollow structural sections for this project were donated by Atlas Tube, Harrow, Ontario, and fabrication services were donated by Walters Inc., Hamilton, Ontario. The financial support of the Natural Sciences and Engineering Research Council of Canada (NSERC) is greatly appreciated.

Symbols

A_w	effective throat area of weld (= $t_w l_w$)
D	overall diameter of the CHS chord
D_b	overall diameter of the CHS branch
F_{EXX}	electrode ultimate strength
F_u	ultimate stress of the CHS; ultimate stress of the plate
F_y	yield stress of the CHS; yield stress of the plate
P	applied force
P_{FE}	failure load in the finite element model
P_a	actual (experimental) load at weld rupture
P_a'	greatest actual (experimental) load sustained by the weld
P_n	nominal/predicted weld fracture load
V_R	coefficient of variation of ρ_R
Z	weld throat dimension when full root penetration is achieved
l	length of the CHS chord member
l_b	length of the CHS branch member
l_h	weld leg measured along the plate; weld leg measured along the CHS chord
l_v	weld leg measured along the CHS branch
l_w	total weld length
t	wall thickness of the CHS chord member
t_b	wall thickness of the CHS branch member
t_p	plate thickness
t_w	weld effective throat dimension
α_R	coefficient of separation (taken to be 0.55)
β	ratio of overall branch diameter to chord diameter
β^+	safety index
δ	chord deformation

ε	engineering strain
ε_T	true strain
ε_e	equivalent (von Mises) strain
ε_{ef}	equivalent (von Mises) strain at rupture for failure criterion
$\varepsilon_{ef,plate}$	equivalent (von Mises) strain at rupture for plate failure criterion
$\varepsilon_{ef,weld}$	equivalent (von Mises) strain at rupture for weld failure criterion
θ	branch inclination angle; angle of loading measured from the weld longitudinal axis for fillet weld strength calculation (in degrees)
ρ	subtended angle around the branch, measured from heel
ρ_R	bias coefficient for the resistance
σ	engineering stress
σ_T	true stress
τ	branch-to-chord thickness ratio
ϕ	resistance factor (associated with the LRFD method)
ϕ_{β^+}	adjustment factor for β^+
Ψ	local dihedral angle (angle between the base metal fusion faces)

References

[1] ISO. (2013). ISO 14346:2013 (E). Static design procedure for welded hollow section joints – Recommendations. Geneva, Switzerland.

[2] Frater, G. S. & Packer, J. A. (1992a). Weldment design for RHS truss connections. I: Applications. Journal of Structural Engineering, American Society of Civil Engineers 118(10): 2784-2803.

[3] Frater, G. S. & Packer, J. A. (1992b). Weldment design for RHS truss connections. II: Experimentation. Journal of Structural Engineering, American Society of Civil Engineers 118(10): 2804-2820.

[4] Packer, J. A. & Cassidy, C. E. (1995). Effective weld length for HSS T, Y, and X connections. Journal of Structural Engineering, American Society of Civil Engineers 121(10): 1402-1408.

[5] McFadden, M. R. & Packer, J. A. (2014). Effective weld properties for hollow structural section T-connections under branch in-plane bending. Engineering Journal, American Institute of Steel Construction 51(4): 247-266.

[6] Tousignant, K. & Packer, J. A. (2015). Weld effective lengths for rectangular HSS overlapped K-connections. Engineering Journal, American Institute of Steel Construction 52 (4): 259-282.

[7] AISC. (2016). ANSI/AISC 360-16. Specification for structural steel buildings. Chicago, IL, USA.

[8] Packer, J. A. & Sun, M. (2011). Weld design for rectangular HSS connections. Engineering Journal, American Institute of Steel Construction 48(1): 31-48.

[9] McFadden, M. R. & Packer, J. A. (2013). Effective weld properties for RHS-to-RHS moment T-connections. Phase 1 Report to the American Institute of Steel Construction. Toronto, Canada: University of Toronto.

[10] McFadden, M. R., Sun, M. & Packer, J. A. (2013). Weld design and fabrication for RHS connections. Steel Construction – Design and Research 6(1): 5-10.

[11] AISC. (2010). ANSI/AISC 360-10. Specification for structural steel buildings. Chicago, IL, USA.

[12] Marshall, P.W. (1992). Design of welded tubular connections – Basis and use of AWS code provisions. Amsterdam, The Netherlands: Elsevier.

[13] ASTM. (2018). ASTM A500/A500M-18. Standard specification for cold-formed welded and seamless carbon steel structural tubing in rounds and shapes. West Conshohocken, PA, USA.

[14] ASTM. (2017). ASTM A370-17a. Standard test methods and definitions for mechanical testing of steel products. West Conshohocken, PA, USA.

[15] AWS. (2015). AWS D1.1/D1.1M:2015. Structural welding code – Steel, 23rd ed., Miami, FL, USA.

[16] Luyties, W. H. & Post, J. W. (1988). Local dihedral angle equations for tubular joints and related applications. Welding Journal, American Welding Society 77(4): 51-60.

[17] Mehrotra, B. L. & Govil, A. K. (1972). Shear lag analysis of rectangular full-width tube connections. Journal of the Structural Division, American Society of Civil Engineers 98(ST1): 287-305.

[18] Swanson Analysis Systems. (2011). ANSYS ver. 14.0. Houston, TX, USA.

[19] Boresi, A. P. & Schmidt, R.J. (2003). Advanced mechanics of materials, 6th ed. NJ, USA: John Wiley and Sons, Inc.

[20] Ling, Y. (1996). Uniaxial true stress-strain after necking. AMP Journal of Technology 5(1): 37-48.

[21] Voth, A. P. & Packer, J. A. (2012). Branch plate-to-circular hollow structural section connections. I: Experimental investigation and finite-element modeling. Journal of Structural Engineering, American Society of Civil Engineers 138(8): 995-1006.

[22] Martinez-Saucedo, G., Packer, J. A. & Willibald, S. (2006). Parametric finite element study of slotted end connections to circular hollow sections. Engineering Structures 28(14): 1956-1971.

[23] Frater, G. S. (1986). Weldment design for hollow structural section joints. M.A.Sc. thesis. Toronto, Canada: University of Toronto.

[24] Ravindra, M. K. & Galambos, T. V. (1978). Load and resistance factor design for steel. Journal of the Structural Division. American Society of Civil Engineers 104(9): 1337-1353.

[25] Fisher, J. W., Galambos, T. V., Kulak, G. L. & Ravindra, M. K. (1978). Load and resistance factor design criteria for connectors. Journal of the Structural Division, American Society of Civil Engineers 104(9): 1427-1441.

[26] Franchuk, C. R., Driver, R. G. & Grondin, G. Y. (2002). Block shear failure of coped steel beams. Proc. Annual Conf. of the Canadian Society for Civil Engineering, Montreal, 5-8 June 2002. 1000-1009.

[27] van der Vegte, G. J. & Makino, Y. (2010). Further research on chord length and boundary conditions of CHS T- and X-joints. Advanced Steel Construction 6(3): 879-890.

[28] Packer, J. A., Choo, Y. S., Shen, W., Wardenier, J., van der Vegte, G. J., & Mustard, T. (2012). CIDECT Report 5BW-2/12. Axially loaded T and X joints of elliptical hollow sections. Geneva, Switzerland: CIDECT.

[29] Kanvinde, A. M. & Deierlein, G. G. (2006). Void growth model and stress modified critical strain model to predict ductile fracture in structural steels. Journal of Structural Engineering, American Society of Civil Engineers 132(12): 1907-1918.

[30] AISC. (2017). Steel construction manual, 15th ed., Chicago, IL, USA.

Figure Captions

Fig. 1 Experimental test specimens: (a) CHS-to-rigid plate connection; (b) CHS-to-CHS X-connection

Fig. 2 CHS-to-rigid plate (a) instrumentation adjacent to the test weld, and (b) typical weld rupture failure mode

Fig. 3 CHS-to-rigid plate FE model with $\theta = 90°$ and key element and mesh details

Fig. 4 Comparison of CHS-to-rigid plate FE and experimental load-displacement responses: (a) test nos. P1, P4 and P6; (b) test nos. P2, P3 and P5

Fig. 5 Effect of branch inclination angle on fillet weld strength in CHS-to-rigid plate connections

Fig. 6 Correlation of AISC 360-16 fillet weld design provisions with 26 weld-critical $\theta = 90°$ CHS-to-rigid plate test results: (a) Section J2.4b [with the $(1.0+0.5\sin^{1.5}\theta)$ factor]; (b) Section J2.4a [without the $(1.0+0.5\sin^{1.5}\theta)$ factor]

Fig. 7 3D weld and section cuts (in Solidworks)

Fig. 8 CHS-to-CHS X-connection experiments: (a) testing arrangement; (b) weld fracture in test no. X5 ($\theta = 90°$); and (c) weld fracture in test no. X9 ($\theta = 60°$)

Fig. 9 Typical strain distributions adjacent to test welds: (a) test no. X7 ($\theta = 90°$), (b) test no. X9 ($\theta = 60°$)

Fig. 10 CHS-to-CHS FE model with $\theta = 90°$

Fig. 11 Comparison of CHS-to-CHS FE and experimental load-displacement responses: (a) test nos. X1, X4 and X5; (b) test nos. X7, X9 and X11

Fig. 12 Correlation of AISC 360-16 Section J2.4a fillet weld design provisions with 268 weld-critical CHS-to-CHS test results